Coordinated Science Laboratory

UNIVERSITY OF ILLINOIS - URBANA, ILLINOIS

PROGRESS REPORT
FOR
MAR. APR. & MAY, 1964

$4.00

COORDINATED SCIENCE LABORATORY
UNIVERSITY OF ILLINOIS
URBANA, ILLINOIS

The research reported in this document was made possible by support extended to the University of Illinois, Coordinated Science Laboratory, under the Joint Services Electronics Program by the Department of the Army, Department of the Navy (Office of Naval Research), and the Department of the Air Force (Office of Scientific Research), and by the Advanced Research Projects Agency under Department of the Army contract

DA-28-043-AMC-00073(E)

the National Aeronautics and Space Administration under Grants

NsG 376 NsG 443 NsG 504

and Department of the Air Force (Office of Scientific Research) contract

AF 49(638) - 1383

July 20, 1964

COORDINATED SCIENCE LABORATORY

SUMMARY OF

PROGRESS REPORT FOR MARCH, APRIL, MAY, 1964

1. Aerospace Group

The results of CSL's first rocket firing in an experiment to measure electron collision frequency in the ionosphere are presented.

2. Surface and Atomic Physics

Experiments on the adsorption of gases on metals are discussed. Advantages of using Auger yield, a function of surface coverage, to study gas adsorption are listed. Apparatus now being constructed to study adsorption, and its associated experimental procedures are described. An apparatus to measure the angular distribution of Auger electrons ejected from tungsten is discussed. The same apparatus can be used for electron diffraction and secondary electron emission measurements. An ultra-high-vacuum rotary-motion feed through, now being constructed, is also described.

3. Computer

Operating statistics for the CDC 1604 and CSX-1 computer are reported. Continued work on heuristic studies in game playing are described. Results of an experimental study of an on-line man-machine dialogue program are reported.

4. Systems

In the switching circuits area, completed studies include the behavior of NOR logic, and the realizability conditions for quasi-linear sequential machines. Further progress is reported on the study of the applications of linear graphs, on probabilistic communication nets, and on the universal compiler. In control systems, new results are reported on the parameter variation problem for a larger class of systems, on a new and more meaningful definition of sensitivity for an optimal system, and on a new solution for the rendezvous problem. In circuits, new results are reported on solutions to nonlinear differential equations, and on the synthesis of the A-matrix for RLC half-degenerate networks.

5. PLATO

Correlations of the variables of the Scientific Inquiry Training lesson (REPLAB) derived from 27 student runs point to a significant discrimination between intuitive and analytical children. REPLAB shows promise of being a tool for the multi-dimensional analysis of the inquiry process. Programming improvements for CATORES have continued as well as preparation of new lesson material. Progress continues on the construction and circuitry of the twenty student station teaching system. The problem of races and firing of adjacencies within the array is being studied in connection with the plasma discharge display tube project.

6. Vacuum Instrumentation

Preliminary results have been obtained in the study of the ionization of oxygen adsorbed on molybdenum. Improvements in the photocurrent suppressor gauge have resulted in improved suppression at lower suppressor voltages. An interesting correlation has been observed between oscillations and negative wall potentials in glass enclosed ionization gauges. The Davis and Vanderslice mass spectrometer is working well and is ready to be used in an experiment. A method for putting lanthanum boride uniformly onto rhenium has been developed. The first experiment on the emission, life, and outgassing characteristics has been finished.

7. Plasma Physics

A new algebraic theory of shock structure provides a sensitive means of comparing analytical and numerical solutions of the Boltzmann equation. A linear induction accelerator has been constructed for the study of run-away in a plasma. Further experiments on the incoherent scattering of microwaves from a plasma indicate the presence of surface modes.

8. High Magnetic Field Superconductors

Work has proceeded on the preparation of Nb_3Sn and the characterization of type II superconductors. The superconducting energy gap in an indium film has been measured as a function of temperature by tunnelling. A new aspect of the Josephson tunnelling effect has been observed.

9. High Voltage Breakdown

Field-emission microscopy is used to observe sites of flickering emission from blunt tungsten tips. The flicker rate is correlated with gas pressure and total emission current. Plans for further study are noted.

10. Evaporated Thin Films

Tin oxide films, formed in air at 600°C, have been found to permanently change their electrical conductivity when exposed to different gases at temperatures higher than 300°C. Stoichometry can be controlled by the use of oxidizing or reducing atmospheres at such temperatures. Vanadium films have been deposited and their superconducting transition examined. An U.H.V. system for epitaxial film growth is now ready for use.

COORDINATED SCIENCE LABORATORY

Personnel

Faculty, Research Associates, and Research Engineers

Alpert, D., Director
Anderson, R.
Ash, R. B.
Barnard, H. M.
Bitzer, Donald
Böhmer, H.
Brown, R. M.
Chen, W. K.
Cooper, D. H.
Cruz, J. B.
Dodd, G.
Elliott, B.
Frauenfelder, H.
  Assoc. Director
Gentry, W.
Gooch, J.
Hicks, B. L.
Kirkwood, B.
Knoebel, H.
Kopplin, J. O.
Krone, H. V.
Kypta, L.
Lee, D. A.
Leichner, E. J.
Lichtenberger, W. W.
  (on leave)
Lüscher, E. (on leave)
Lyman, Elisabeth
Lyman, Ernest
Mayeda, W.
Mueller, T.
Peacock, R. N.
Perkins, W.
Ponzo, P.
Propst, F.
Prothe, W. C.
  Asst. to Director
Raether, M.
Resh, J.
Rohrer, R.
Satterthwaite, C. B.
Schuemann, W. C.
Seshu, Sundaram
Simonelli, L.
Skaperdas, D.
Slottow, H. G.
Sobral, M.
Steinrisser, F.
Stifle, J.
Tomaschke, H. E.
Trogdon, R.
Van Valkenburg, M.E.
  Assoc. Director
Voth, B.
Wax, Nelson

Research Assistants

Aggarwal, J. K.
Barger, A. R.
Batcher, K.
Bernstein, R.
Blomme, R.
Chang, Herbert Y.
Chen, W. K.
Cooper, T.
Craford, M.
Crowder, James
Cummings, James
Dervisoglu, A.
DeWan, E.
Franz, Frank
Gieseking, D.
Hosken, R.
Jacobs, J. T.
Jenks, Richard
Lie, T.
Manning, E.
Mendel, C.
Morgan, Lezlie
Murata, T.
Onaga, K.
Piper, Thomas
Secrest, M.
Smith, Margaret
Snyder, D. P.
Sobral, M.
Tahim, G.
Tibbets, G.
Toepke, I.
Werner, R.
Willson, R. H.
Zelac, R.

Fellows

Agashe, S.
Carr, W.
Paul, A.
Rain, D.
Sain, M.
Win, S.

Accountant

Klein, N.

Secretary

Gschwendtner, J.

Typists and Stenos

Barnard, M.
Corray, R.
Harris, M.
Long, W.
McDonald, R.

Instrument Makers

Beaulin, W. E.
Merritt, K. E.
Zackery, R. L.

Glassblower

Lawrence, W.

Phys. Sci. Staff Asst.

Thrasher, W.

Storekeepers

Drews, C. E.
Lofton, C.

Electronic Technicians

Casale, T.
Coad, D. E.
Cooper, G.
Crawford, G.
Deschene, D. R.
Holy, F. O.
Jordan, H.
Knoke, J. G.
Merrifield, F.
Popeney, T. W.
Roberts, G.
Schmidt, W.
Simpson, L.
Streff, L. W.
Turpin, F. G.

Accounting Clerk

Hanoka, N.
Potter, R. E.

Photographer

Fillman, W.

Draftsmen

MacFarlane, R. F.
Tewes, A. F.

Laboratory Mechanics

Bouck, G.
Burr, J. G.

Electronics Engr. Asst.

Carter, E. N.
Gardner, O. E.
Hedges, L.
Neff, E. H.
Vassos, N.

Res. Lab. Shop Supr.

Bandy, L.

Student Assistants

Alper, G.
Arnold, C.
Arfman, J.
Chilton, S.
Downs, J.
Edelheit, L.
Etienne, L.
Gobberdiel, J.
Johnson, M.
Jones, A.
Klein, W.
Klingbiel, R.
Lacina, C.
Metze, V.
Nagel, D.
Nash, R.
Riddle, G.
Ries, R.
Robinett, D.
Samson, C.
Sandorfi, G.
Singer, S.
Toepke, I.
Ulbrich, N.
Walker, M.
Whitney, R.

PUBLICATIONS AND REPORTS

1. Journal Articles Published or Accepted

H. Barnard, "Note on Completely Partitionable Terminal Capacity Matrices," IEEE Trans. on Circuit Theory (in press).

W. K. Chen, "On Signal-Flow Graphs," Proc. IEEE, (to appear).

W. K. Chen, "The Inversion of Matrices by Flow Graphs," J. Soc. for Indust. and Appl. Math., (in press).

J. B. Cruz, Jr., "Progress in Time-Varying and Active Circuit Theory," IEEE Trans. on Circuit Theory, vol. CT-11, pp. 6-10; March, 1964.

J. B. Cruz, Jr., and W. R. Perkins, "A New Approach to the Sensitivity Problem in Multivariable Feedback System Design," IEEE Trans. on Automatic Control, vol. AC-9, July, 1964.

A. Dervisoglu, "Bashkow's A-Matrix for Active RLC Networks," IEEE Trans. on Circuit Theory, (in press).

H. W. Knoebel, "The Electric Vacuum Gyro: Pinpoint for Polaris Launching," Control Engineering, February, 1964.

W. R. Perkins and J. B. Cruz, Jr., "The Parameter Variation Problem in State Feedback Control Systems," Trans. ASME, 1965.

R. A. Rohrer, "Analytical Mechanics and the Analysis of Linear Time-varying Networks," Journal of the Franklin Institute, (to appear, August, 1964).

M. Raether and D. Bitzer, "Polarity Coincidence Detector for the Measurement of Very Small Signal-to-noise Ratios," Rev. Sci. Instr., (in press).

M. E. Van Valkenburg, "Progress in Passive Circuit Theory--1960-63," IEEE Trans. on Circuit Theory, vol. CT-11, pp. 3-6, March, 1964.

2. Meeting Papers

D. L. Bitzer and J. A. Easley, Jr., "PLATO: A Computer-Controlled Teaching System", 19th National Conference on Higher Education, Association for Higher Education (NEA), April, 1964, Chicago, Illinois.

D. L. Bitzer and J. A. Easley, Jr., "PLATO: A Computer-Controlled Teaching System", Department of Audiovisual Instruction National Convention (NEA), April, 1964, Rochester, New York.

J. B. Cruz, Jr. and W. R. Perkins, "The Sensitivity of General Multivariable Feedback Systems", International Conference on Microwaves, Circuit Theory, and Information Theory; September 7-11, 1964, Tokyo, Japan.

W. Mayeda and M. E. Van Valkenburg, "Properties of Lossy Communication Nets", International Conference on Microwaves, Circuit Theory, and Information Theory; September 7-11, 1964, Tokyo, Japan.

W. R. Perkins and J. B. Cruz, Jr., "Sensitivity Operators for Linear Time-Varying Systems", International Symposium on Sensitivity Analysis, August 31-Sept. 5, 1964, Dubrovnik, Yugoslavia.

R. A. Rohrer and M. Sobral, Jr., "Sensitivity considerations in optimum system design", National Electronics Conference, Oct., 1964, Chicago, Illinois.

3. Technical Reports

R-184 Self-Directed Inquiry in Clinical Nursing Instruction by means of the PLATO Simulated Laboratory; Maryann Bitzer.

R-195 Final Report, CSL Electric Vacuum Gyro; D. Skaperdas and H. Knoebel.

R-196 Optimal Linear Switching for Singular Linear Systems; R. A. Rohrer and M. Sobral, Jr.

R-197 Lectures on Magnetohydrodynamics; V. C. A. Ferraro.

R-198 Heart Rate Correlates of Insight; R. A. Avner.

R-199 Optimal Singular Solution for Linear, Multi-Input Systems; R. A. Rohrer and M. Sobral, Jr.

R-200 Properties of Lossy Communication Nets; W. Mayeda and M. E. Van Valkenburg.

R-201 Electron Collisions in Neon Plasma; C. L. Chen.

R-202 Spin Relaxation of Optically Pumped Cesium; Frank Franz.

R-203 Application of Linear Graphs to Electrical Networks, Switching Networks and Communication Nets; W. Mayeda.

R-205 Speed Independent Nor Realizations; Kenneth E. Batcher.

R-206 The Scattering Matrix: Normalized to Complex n-Port Load Networks; R. Rohrer.

R-207 On an Improved Diagnosis Program; S. Seshu.

R-208 A Performance Measure for Game-Playing Programs; E. Manning.

R-209 Synthesis of Probabilistic Communication Nets; H. Barnard.

R-211 Some Applications of Linear Graphs; W. K. Chen.

R-212 Properties of Classes of Paths; W. Mayeda.

TABLE OF CONTENTS

CONTENTS (Continued)

CONTENTS (Continued)

1. AEROSPACE GROUP

H. W. Knoebel
D. O. Skaperdas
B. D. Kirkwood
H. V. Krone
J. D. Gooch
D. A. Lee
W. C. Prothe
R. W. Anderson

On April 16, 1964, the Coordinated Science Laboratory of the University of Illinois fired its first rocket at Wallops Island, Virginia, in a series of experiments probing the ionosphere conducted under a synoptic IQSY Program which is directed by Dr. Sidney Bowhill. (See Fig. 1.1, 1.2, and 1.3.) The experiment was very successful. It utilized part of the 60 pound payload of a Nike-Apache rocket which was sent 105 miles into the atmosphere. The purpose of this experiment was to measure the differential absorption and Faraday rotation for the determination of electron collision frequency in the D-region. This section will describe the novel system used to make these measurements and will present the data obtained from them.

At Wallops Island, the CSL antenna and van, which contained all of the ground-based equipment, was located approximately two miles southwest of the rocket launching site, one mile southwest of the University of New Mexico telemetry station, and 11 miles south of the main base telemetry station. Since the experimental system contained a feedback loop closed via the CSL van, the rocket, one of the telemetry stations, and back to the van, special lines had to be laid between the van and the two stations, one of which was used as a backup. Provisions were made to close the feedback loop via whichever of the two telemetry stations obtained the better signal from the rocket. As it turned out

Fig. 1.1. Rocket payload suspended from helicopter during system tests at the CSL antenna site, Champaign, Illinois.

Fig. 1.2. Nike-Apache Rocket 14.143 on the launching pad at Wallops Island, Virginia. The technician at right is holding the umbilical cord.

Fig. 1.3. Nike-Apache Rocket 14.143 at moment of launch, April 16, 1964.

during the rocket trajectory, the New Mexico station delivered a much better signal to the CSL van because of the shorter telephone line.

The electron collision frequency can be computed from measurements of the electron density and of the relative absorption of two oppositely circularly polarized radio waves (ordinary and extraordinary) propagated through the ionosphere in the direction of the earth's magnetic field. The differential absorption gives a measurement of $\int N\nu dz$ where N is the electron density, ν is the collision frequency, and z is the height. The electron density can be obtained from the relative polarization angle between the ordinary and extraordinary waves (Faraday rotation), this quantity being proportional to $\int N dz$. The electron density can also be measured independently by means of a probe on the rocket. The relative or differential absorption and total absorption, apart from the inverse square law attenuation, are functions of frequency. It is desirable to choose a frequency low enough to yield significant amounts of differential absorption and yet have enough extraordinary wave signal left to measure Faraday rotaiton. Since it is difficult to predict well in advance the level of ionospheric ionization, and since the simultaneous success of both measurements is critically dependent on the choice of frequency, provision was made for two sets of equipment tuned in advance to different frequencies in the two to four megacycles range.

Two oppositely, circularly polarized waves differing by 500 cps in frequency were simultaneously transmitted from the antenna array. Looking up into the sky along the earth's magnetic field, the counterclockwise wave is the extraordinary wave in the northern hemisphere.

The two waves resolve into a plane polarized wave whose direction of polarization rotates at one-half the difference frequency, or 250 cps. A magnetic dipole receiving antenna located in the rocket receives an amplitude modulated (500 cps) signal resulting from the scan rotation of the polarization (one cycle for each half revolution). The phase of this modulation measured with respect to the beat at the transmitting antenna gives a measure of twice the apparent angular difference in polarization of the two antenna systems. This angular difference includes the integrated effect of both Faraday rotation and the physical rotation of the rocket receiving antenna due to rocket spin, which is independently measured by magnetic sensors and subtracted from the data to obtain the integrated Faraday rotation.

In the absence of differential absorption the two oppositely, circularly polarized waves arrive at the rocket antenna with the same intensity and thus combine at the receiver to produce a rectified sinusoidally modulated output having sharp nulls for each 180^{o} of scan rotation. The presence of differential absorption reduces the sharpness of these nulls so that the degree of modulation of this signal gives a measure of differential absorption while, at the same time, the phase of the modulation gives a measure of twice the Faraday rotation.

The CSL system was designed to operate in any of three modes of increasing complexity. The least complex mode maintains the transmitted ordinary and extraordinary circularly polarized waves at the same power. This method makes the measurement of Faraday rotation difficult when the differential absorption becomes large at the higher altitudes resulting in decreased signal modulation. Furthermore, the receiver

output versus input characteristics must be accurately known in order to measure the differential absorption.

The second mode is to mechanically sweep the ordinary (clockwise looking up) transmitted wave output power by means of an attenuator, traversing the entire range about once each second. This would insure appropriate measuring conditions at least twice each second, corresponding to data points no more than one kilometer apart.

The third and most complex mode, and the one which was used successfully on our first experiment, is to control the extraordinary wave transmitted power by means of an attenuator activated by feedback of the received signal telemetered from the rocket, keeping the ordinary transmitted power constant. As differential absorption appears, the attenuation would be continuously reduced by a servomechanism to maintain the modulation of the received signal at a fixed 32% corresponding to a 10 db difference in the intensity of the two received wave components. The attenuator settings are continuously recorded along with the telemetry data, enabling subsequent determination of the differential absorption.

Fig. 1.4 is a block diagram of the entire system used for the April 16 rocket experiment. The CSL van equipment is shown within the dotted lines at the left. The system was previously described in CSL Quarterly Progress Report for Dec. 1963, Jan., Feb., 1964. The attenuators and drive mechanism controlling the ordinary and extraordinary wave transmitted power are shown in Fig. 1.5 a,b. In Fig. 1.5a the gear box is opened for inspection. One of the two knobs shown controls the overall output power and the other knob controls the differential

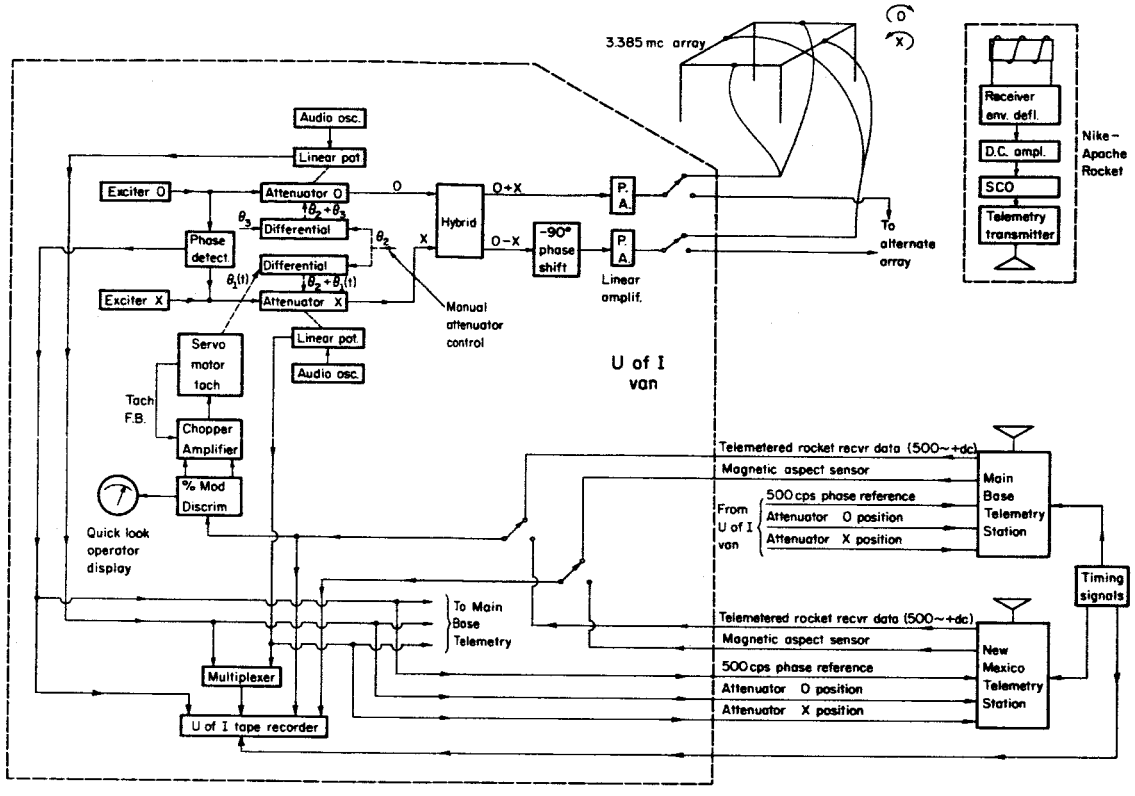

Fig. 1.4. Block Diagram of the CSL Ionosphere Experiment

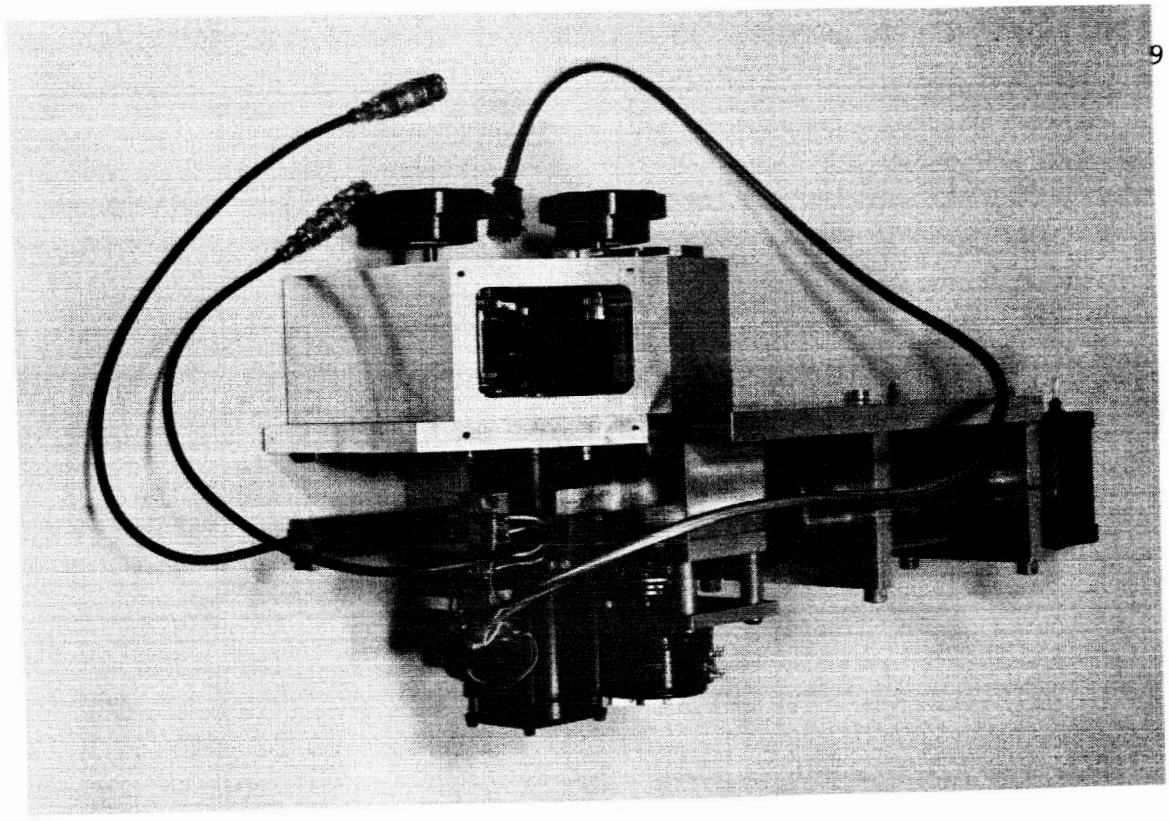

(a)

(b)

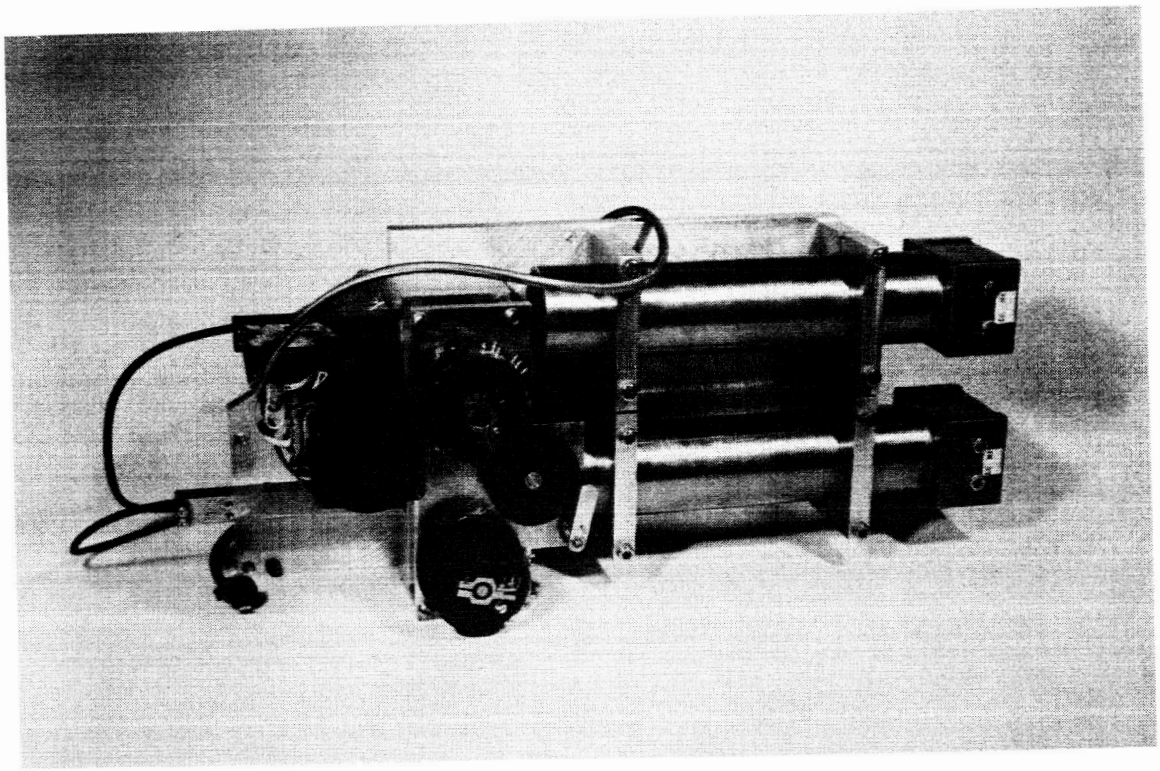

Fig. 1.5. Waveguide-Beyond-Cutoff Attenuators and Servo Drive Mechanism.

power of the oppositely circularly polarized waves. The waveguide-beyond-cutoff attenuators are the two brass cylinders with matching networks which are enclosed within the attached boxes at the right. (Fig. 1.5b). Also visible are the linear potentiometers which are geared to their respective attenuators.

Fig. 1.6a shows the ferrite-rod rocket antenna before potting and 1.6b after potting and in its rocket support assembly. A fiberglass cylinder surrounds this assembly. Fig. 1.7 shows the transistorized, crystal-controlled superheterodyne receiver developed for CSL by Space Craft, Inc., of Huntsville, Alabama.

The Nike-Apache rocket used in CSL's first experiment, designated as Number 14.143, reached an apogee of 105 statute miles and a horizontal range of 110 miles with a flight time of 406 seconds. All of the differential absorption and Faraday rotation during the ascent took place from about 60 seconds to 90 seconds after launch. Apogee occurred at 205 seconds.

A general picture of the experiment can be seen in Fig. 1.8 which shows five recorded signals of interest during the entire rocket flight. The signals at the top and bottom edges are universal time signals. The second signal from the top is the telemetered rocket receiver output consisting of a dc component and 500 cps difference frequency modified by the rocket spin frequency and Faraday rotation. The next lower signal is the telemetered magnetic aspect sensor which measures the transverse component of the earth's magnetic field. Each period of this sinusoidal signal represents one rotation of the rocket. The next lower signal represents the magnitude of the extraordinary

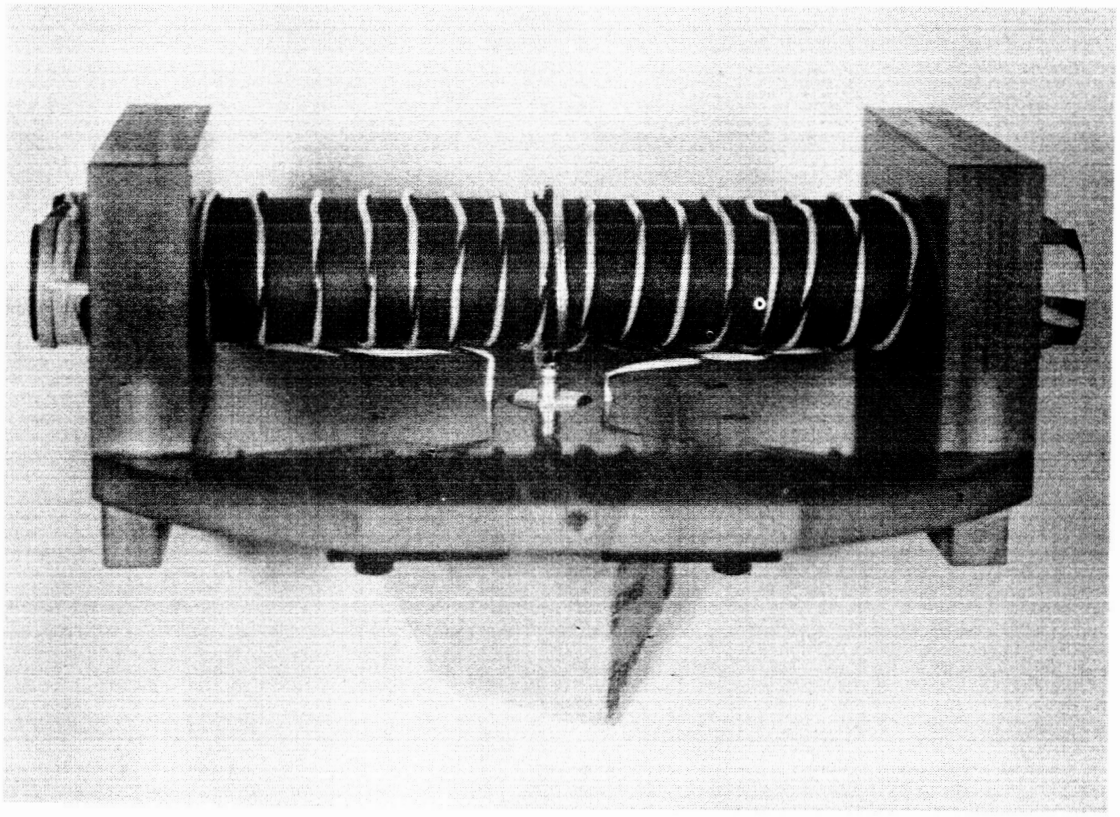

(a)

(b)

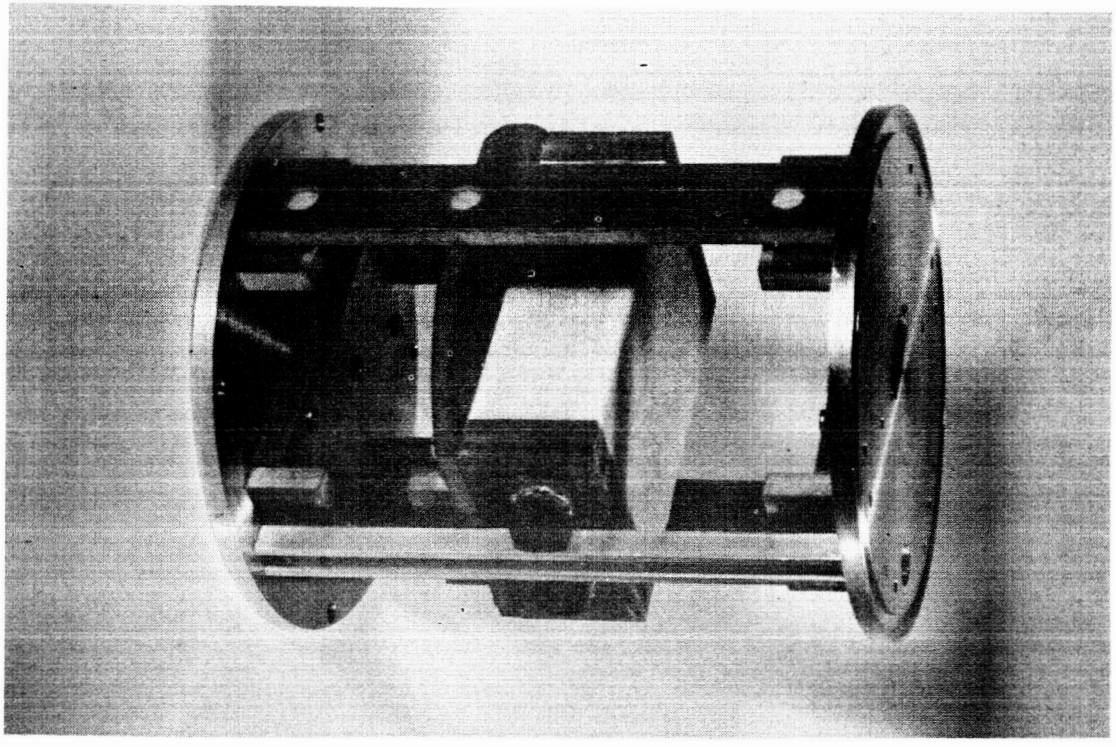

Fig. 1.6. Ferrite Rod Rocket Antenna

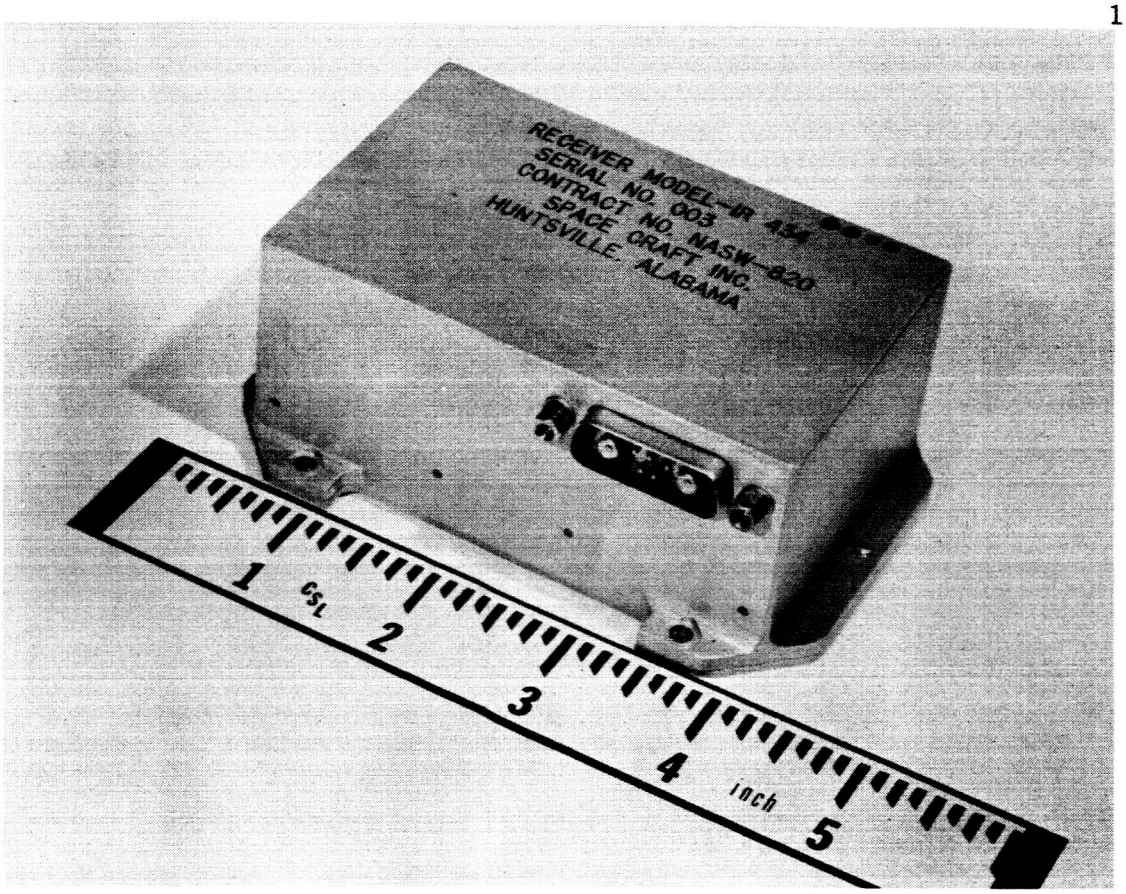

Fig. 1.7. Rocket Receiver.

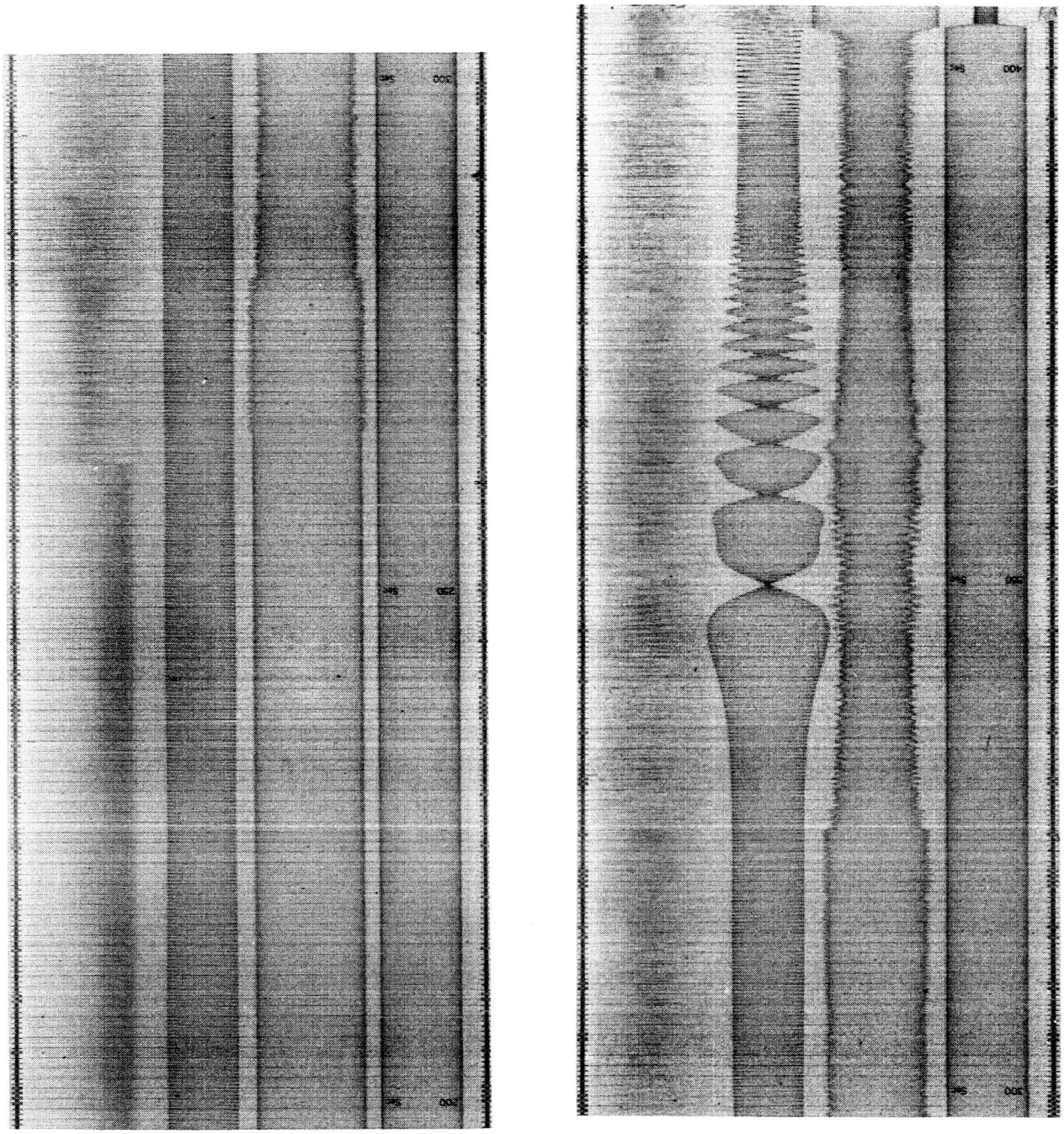

Fig. 1.8. Some of the Recorded Signals of Rocket Flight 14.143. The four panels (see also facing page) constitute a continuous record.

wave transmitted power. It consists of a 200 cps audio signal output of a linear potentiometer coupled to the servo-controlled attenuator. The second signal from the bottom represents the magnitude of the ordinary wave transmitted power as indicated by the amplitude of a 100 cps audio signal. The distance between vertical lines represents one second of time. It is seen from Fig. 1.8 that the ordinary wave power was kept constant (at about 10 watts) during the entire flight. The initial extraordinary wave power was at about 1 watt. Time of launch (t = 0 sec) can easily be discerned from the magnetic aspect sensor signal, as the rocket begins to spin at an increasing rate. No particular effect is observed at t = 3.5 sec where the Nike first stage burned out. However, at about t = 20 sec, when the second stage (Apache) fired, a slowdown of the rocket spin occurred, a usual phenomena which cannot be explained by the Wallops Island personnel. At t = 28 sec, the Apache stage burned out and a precession of the rocket about its spin axis appears. At t = 40 the ejectable doors covering an aperture used in a separate radiation experiment conducted by GCA were released. The rocket precession damped out at about 70 sec, at which time the rocket spin rate stabilized at 6 rps. Apogee occurred at 205 sec and at t = 330 sec the rocket appears to have reentered the earth's atmosphere at a point where frictional drag caused it to tip over and descend like a precessing bomb. At t = 340 sec the magnetic aspect sensor axis was perpendicular to the earth's magnetic field, resulting in zero signal output. At t = 403 the rocket hit the ocean, resulting in loss of signal.

Returning to the other signals, at -60 sec < t < 0 sec, the servo loop was closed, with attenuator X at 32 db below one kilowatt and attenuator 0 at 20 db below one kilowatt. At t = 0, there was a

sudden change of the rocket receiver signal, causing a servo impulse which quickly damped out, probably due to the rocket blast. Fig. 1.9a is a time enlarged view of this event. In these figures, one second of time is represented by the light vertical lines (see Fig. 1.9b). In Fig. 1.9 are also shown, as the second and third records from the top, the sum of the rocket receiver signal (fourth from top) with the 500 cps reference signal and with the 500 cps reference signal phase shifted 90^{o}. These traces, together with the magnetic aspect sensor trace (fifth from top), are used to measure Faraday rotation. In Fig. 1.9a (t = 0), the rocket has not yet made one revolution. At t = 28 to 40 sec the rocket receiver was cut off in order to obtain a calibration signal. The signal in this interval represents zero dc receiver output voltage. In the interval t = 60 to 90 seconds, the output of attenuator X is increasing, showing that differential absorption is taking place. Fig. 1.9b is representative of the recorded signals near t = 66 sec, where the rocket is at an altitude of 77 km. The magnetic aspect sensor trace indicates that the rocket was spinning at about 6 cps. The rocket receiver difference frequency shows a modulation due to the rocket spin and a standing wave caused by reflection of the extraordinary wave at a higher altitude. At t = 85 sec (100 km) Fig. 1.9c shows the standing wave ratio getting larger. At t = 90 sec (106 km) the differential absorption (and Faraday rotation) suddenly stop, signifying a reflection of the extraordinary wave at this point. A further time expansion of Fig. 1.9d shows a sudden phase reversal of the receiver difference frequency, corroborating this reflection. At this altitude the maximum system resolution between clockwise and counterclockwise circularly polarized waves has been

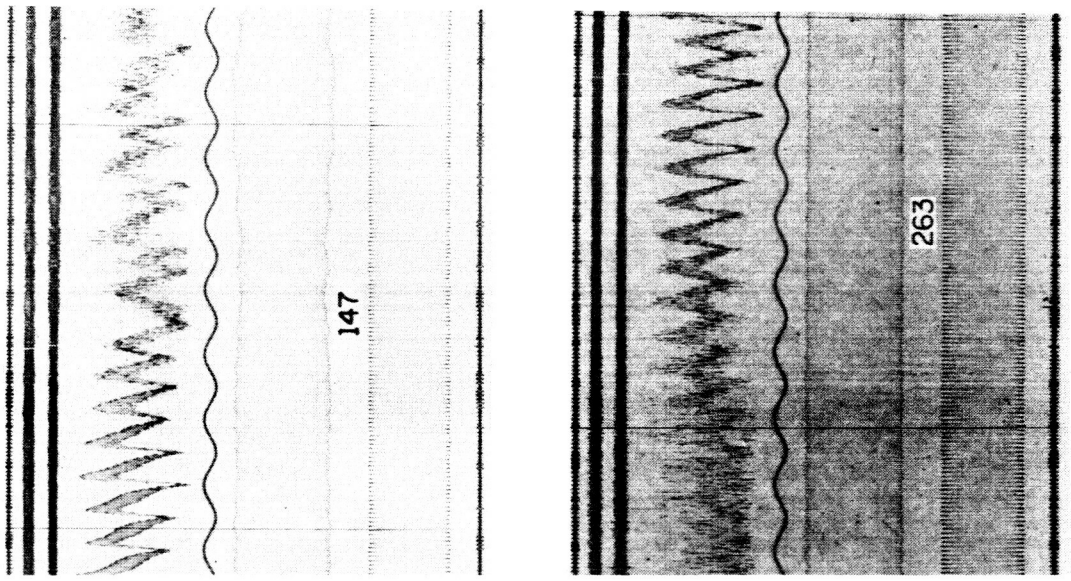

(g) (h)

(c) (d)

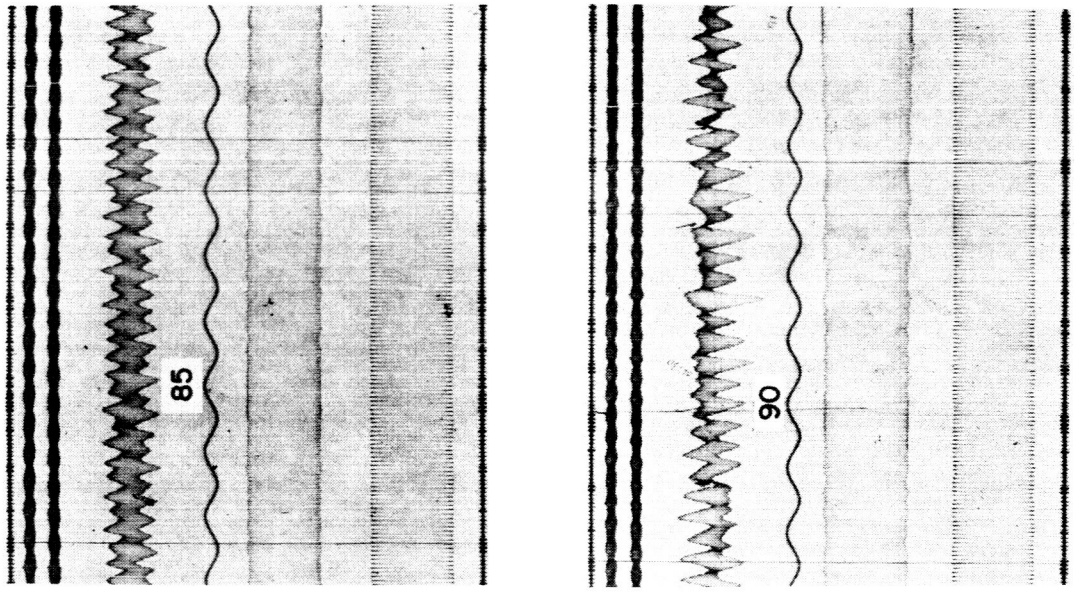

Fig. 1.9. Enlarged Views from Fig. 1.8.

reached (about 26 db). Above this altitude only the standing waves are of interest. Fig. 1.9e shows the rocket receiver modulated by the standing wave at t = 110 sec (125 km). The receiver difference frequency in this case is due to some ordinary (clockwise) component being radiated at the extraordinary frequency due to a slightly elliptically polarized antenna system. It is interesting to note that at all altitudes higher than the extraordinary reflection level (106 km), the receiver difference frequency suddenly dropped to the value of 500 cps, the value it had before launch. This can be explained if the two circularly polarized waves are rotating in the same sense (clockwise in this case) thereby nullifying the effect of rocket spin.

A comparison of the standing wave wavelengths in Fig. 1.9b and 1.9d shows the effect of the decreasing index of refraction and consequent increasing phase velocity of propagation with increasing altitude. At t = 120 sec (134 km) a zero beat of the rocket receiver modulation envelope caused by the rocket spin and the standing wave pattern can be seen in Fig. 1.8. The effect of a very large standing wave ratio on the rocket receiver output is shown in Fig. 1.9f at t = 141 sec (149 km). Since the AGC feedback loop has an integrator at the standing wave frequency, the receiver closed loop differentiates the standing wave pattern (full wave rectified sine wave) to give the waveform shown in Fig. 1.9f. At t = 147 sec (152 km) a second reflection layer occurs. In Fig. 1.9g it is seen that the rocket receiver signal suddenly becomes noisy. One second later the second calibration signal occurred for a total of 12 sec, masking the presence of a third reflection layer. This was later observed during the descent and is shown in Fig. 1.9h. At

this point the system servo loop was opened. During the descent the combination of a large standing wave ratio and rocket precession and tilt made the data extremely noisy. However, at t = 262 sec (153 km) the rocket again broke through the third reflection level (Fig. 1.9h) and the system servo loop was again closed a few seconds later as seen by the jittering attenuator X record. The second reflection level with identical rocket receiver characteristics as in Fig. 1.9g was again passed at t = 281 sec (142 km). At this time attenuator X jumped to a new level and stayed there until the differential absorption region starting at t = 325 sec (102 km) was reached, at which point the extraordinary power started to decrease. Nine seconds later the rocket started to tumble, hitting the ocean at t = 406 sec. At this point the system servo loop was broken and the two attenuators were driven against their stops, as shown in Fig. 1.8.

The differential absorption and Faraday rotation versus altitude is shown in Fig. 1.10. A total differential absorption of about 20 db and a Faraday rotation of about 14 cycles was observed. The Faraday rotation data was obtained by three different methods of data analysis, the results closely agreeing. One method was fully automatized, using CSL's recording tape of the flight data and two phase meters, with the Faraday rotation vs. time of flight indicated on a pen recorder. A second method consisted of manually counting the total number of cycles of the rocket receiver difference frequency, up to a given time and subtracting from it the total number of cycles of the 500 cps phase reference and the rocket spin frequency up to that same time. The third method consisted of counting the number of cycles of the modulation

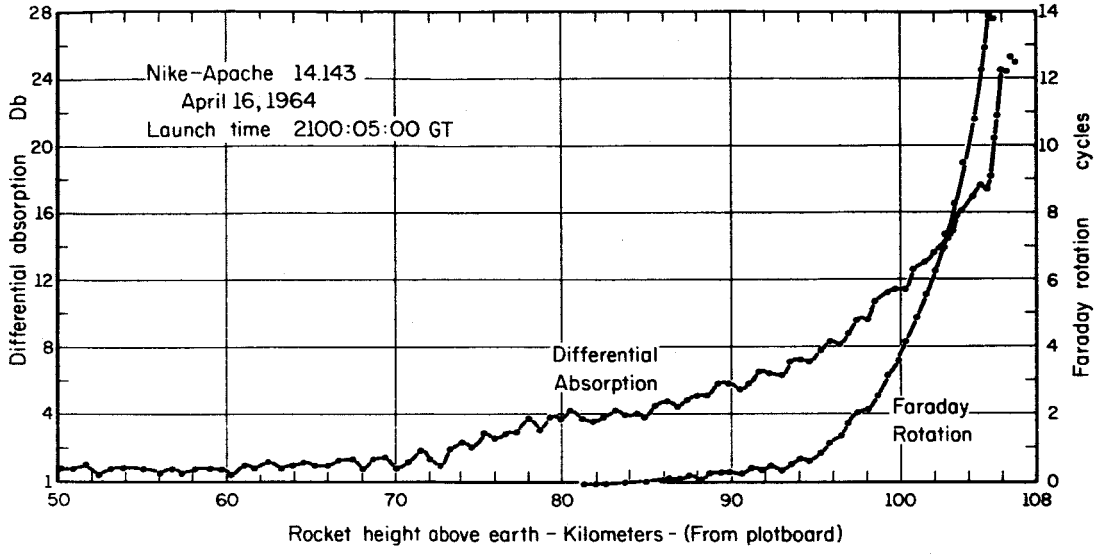

Fig. 1.10. Differential Absorption and Faraday Rotation vs. Rocket Height for Flight 14.143.

envelope of the second or third traces from the top in Fig. 1.9 up to a given point and subtracting the total number of cycles of the rocket spin frequency up to that same point.

The probable error for measuring Faraday rotation by the latter two methods is about 0.1 cycle. However, the probable error of the first method is about 5 degrees at the low values, increasing as the rate of rotation increases. Efforts are now being made to reduce this error to about one degree. The probable error in the differential absorption method is about 0.5 db due to the noise pick-up on the attenuator X and 0 data lines.

The computations for collision frequency are currently being done under Professor Sidney Bowhill's direction.

D. O. Skaperdas
H. W. Knoebel

2. SURFACE AND ATOMIC PHYSICS

Surface:

F. Propst
G. Tibbetts
T. Piper
F. Hummel
T. Cooper

Atomic:

H. Frauenfelder
F. Franz

2.1 A New Study of the Adsorption of Gases on Tungsten

Much of the work that has been done on the adsorption of gases on metallic surfaces has suffered from the inherent limitations of the standard methods. Coverage, θ, the fraction of possible adsorption sites which are filled by gas atoms, is the quantity whose measurement is most necessary.

When gas is adsorbed on the surface, there is a realignment of the electronic bonds on the surface metal atoms. The resulting change in work function, closely related to θ, may then be measured by many methods, all of which are rather difficult. Field emission studies have given direct, but difficult to reproduce, information about adsorbed surface atoms. Electron diffraction also has been successfully used; however, this technique fails when the scattering factor of the adsorbed species is much smaller than that of the substrate, or when the adsorbed gas replicates the crystallographic structure of the substrate.

Probably the best information to date has been obtained by flashing a tungsten filament to drive off the adsorbed gases and then measuring the consequent pressure rise within the system.[1] This

[1] Ehrlich, Jour. Chem. Ph. 34 No. 1, p. 29.

method requires extreme precautions in relating the pressure rise to θ. Furthermore, as long, thin filaments are used, specific crystalline faces are not available. Since field-ion-microscope studies indicate that the adsorption of gases has different characteristics on the different crystal faces, this method leaves many questions unanswered.

Migration of the gas atoms off the end of the filament when desorptive heating has begun can also decrease the amount of gas evolved, thus decreasing the value obtained for the desorption constant.

We intend to use secondary emission of electrons by low energy incident ions to measure the degree of surface coverage. In the clean surface case, He^+ ions incident on tungsten interact with two electrons from the metal's conduction band. One of the electrons drops into the empty level, neutralizing the He^+ ion, and the other adsorbs the energy released in the process, ultimately being ejected from the metal in about ½ of the cases. The ratio,

$$\gamma = \frac{\text{electrons ejected}}{\text{incident ions}}$$

is called the "Auger yield." Propst[2] has suggested that when gases are absorbed on the tungsten, the secondary electrons attempting to escape the metal are scattered back into the metal with a probability dependant on the coverage. Experimentally, θ is found to decrease almost linearly with increasing coverage until there is about one monolayer of adsorbed gas on the surface.

Thus, an observation of γ gives a direct and sensitive measure of θ, since the amount of high energy secondaries may decrease by a

---

[2] Propst and Luscher, PR 132, No. 3, pp. 1037-1046, 1963.

factor of 3 or more with adsorption of one monolayer of gas. Since only a small area of tungsten need be observed, it is possible to use single crystal material.

The apparatus shown in Fig. 2.1 is now under construction. Basically, we will use an electron impact Helium ion source, leading to a cylindrical lens which focuses the ions onto the target. The target is a single-crystal tungsten ribbon mounted on two heating leads which pass directly into a liquid nitrogen cooling bath. If the ion current is held constant by a feedback loop to the ion source, then γ is directly proportional to the current from the collector electrode.

The desorption process is analagous to the problem of a particle vibrating with a frequency ν in a potential well of depth E_B. An approximation to the escape probability will be,

$$\beta(T) = \nu e^{-E_B/kT}$$

If there are several possible types of bonding wells available on the surface, as is suspected,

$$\beta(T) = \sum_i \nu_i \, e^{-E_{Bi}/kT}$$

We will illustrate the experimental technique by considering desorption of a monatomic gas from the surface. First we flash the target clean and allow it to cool at time t_o (Fig. 2.2). At time t_1 the target has cooled, so that gas can be admitted, and the target exposed until the coverage increases to θ_o and the change in yield is $\Delta\gamma_o$. The gas flow is stopped at t_2. Now, at time t_3 the target temperature is increased to temperature T_1 or T_2 so that thermal desorption begins.

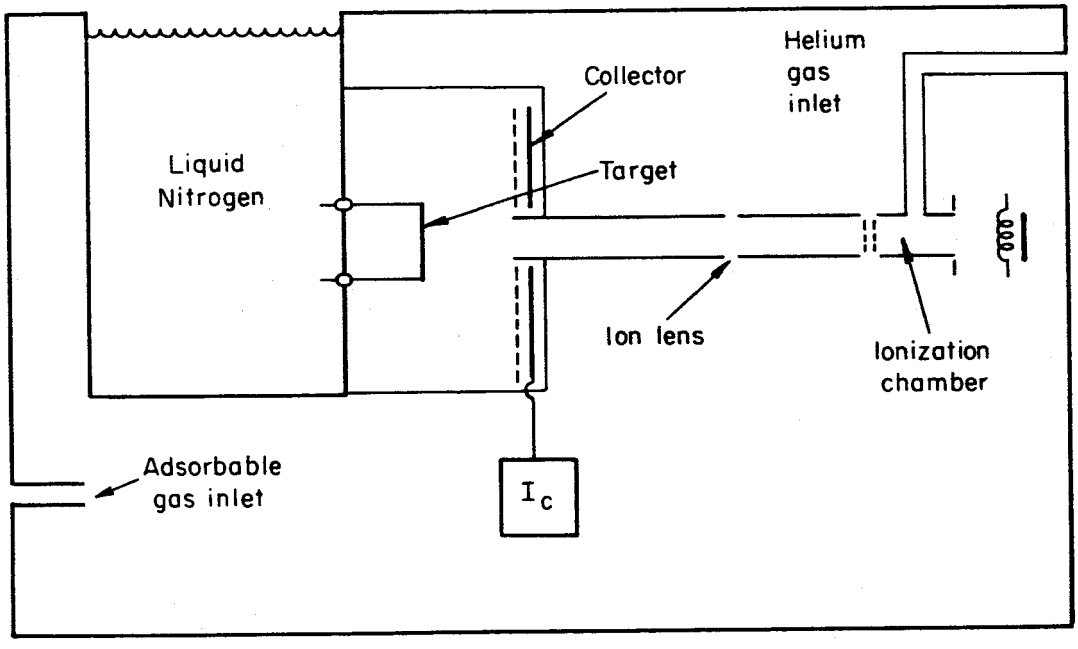
Helium
gas
inlet
Collector
Liquid
Nitrogen
Target
Ion lens
Ionization
chamber
Adsorbable
gas inlet
I_c

Fig. 2.1.

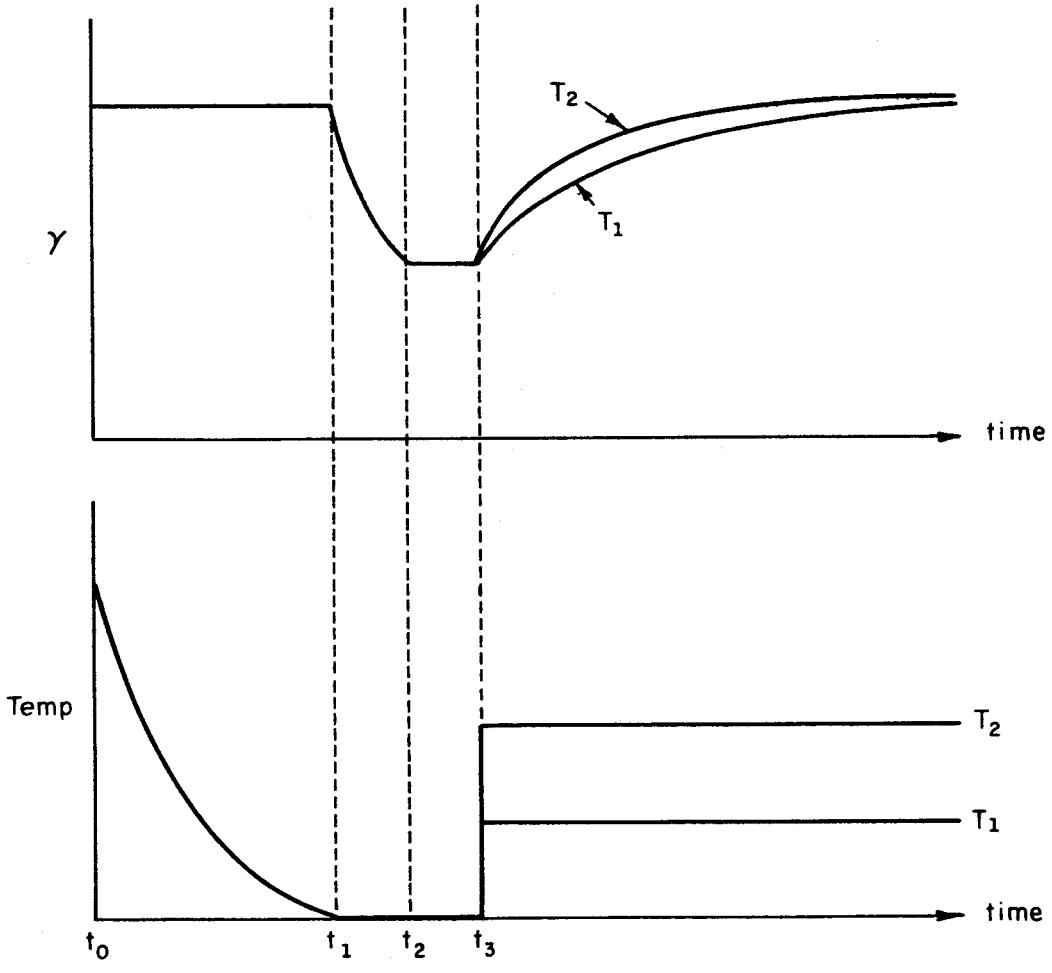

Fig. 2.2.

As desorption continues, the values of the yield in both cases approach the clean surface value. We define the desorption coefficient $\beta(T)$ in this case by the equation,

$$\frac{d\theta}{dt} = -\beta(T)\,\theta$$

so that

$$\beta(T) = (1/t)\ln(\theta_o/\theta) = (1/t)\ln(\Delta\gamma_o/\Delta\gamma)$$

Thus by plotting $\ln(\Delta\gamma_o/\Delta\gamma)$ vs. t, we can find β from the slope. Non-linearities in the slope will reveal complexities in β, such as the small variation of β with θ.

This plotting procedure gives us one value of $\beta(T)$. By repeating the operation for all temperatures, T_1, T_2, ..., we will be able to construct the entire behavior of β with respect to T, and check with the simple model we have used to determine E_B and υ. We hope to be able to determine the number of bonding states and their energies from this information.

Finally, we note that this technique can be applied to various types of desorption, such as electron impact desorption, photodesorption, and ion sputtering.

2.2 Angular Distribution of Auger Electrons

Although the Auger neutralization effect[3] has been studied extensively during the last few years, a number of important questions still remain unanswered. Among these are:

---

[3] C.S.L. Technical Report, R-161

(1) What is the angular distribution of ejected electrons?

(2) To what degree does the interaction between Auger and conduction band electrons influence the effect?

(3) To what degree does the crystal structure influence the effect?

(4) How does the effect depend on the angle of incidence of the ion beam?

An apparatus is being designed to perform three types of surface studies on a given crystalline surface in situ. The three measurements are:

(1) Auger neutralization

(2) Electron diffraction

(3) Secondary electron emission.[4]

It is hoped the correlation of these three types of measurements will provide definitive answers to the above questions. This study, in conjunction with the experiment described in the previous section, should also provide a more coherent picture of surfaces and surface interactions.

The apparatus is shown schematically in Fig. 2.3. Low energy (<200 ev.) ions or electrons impinge on a single crystal, tungsten target.[5] The scattered or ejected electrons pass through a slot in the shield and are collected by a Faraday cage collector. Two grids attached to the collector make possible the direct measurement of the energy

---

[4] H. Bruining, Physics and Applications of Secondary Electron Emission, Pergamon Press, New York, 1954.

[5] G. Tibbetts and F. M. Propst, R. S. J. 34, No. 11, pp. 1268-1269.

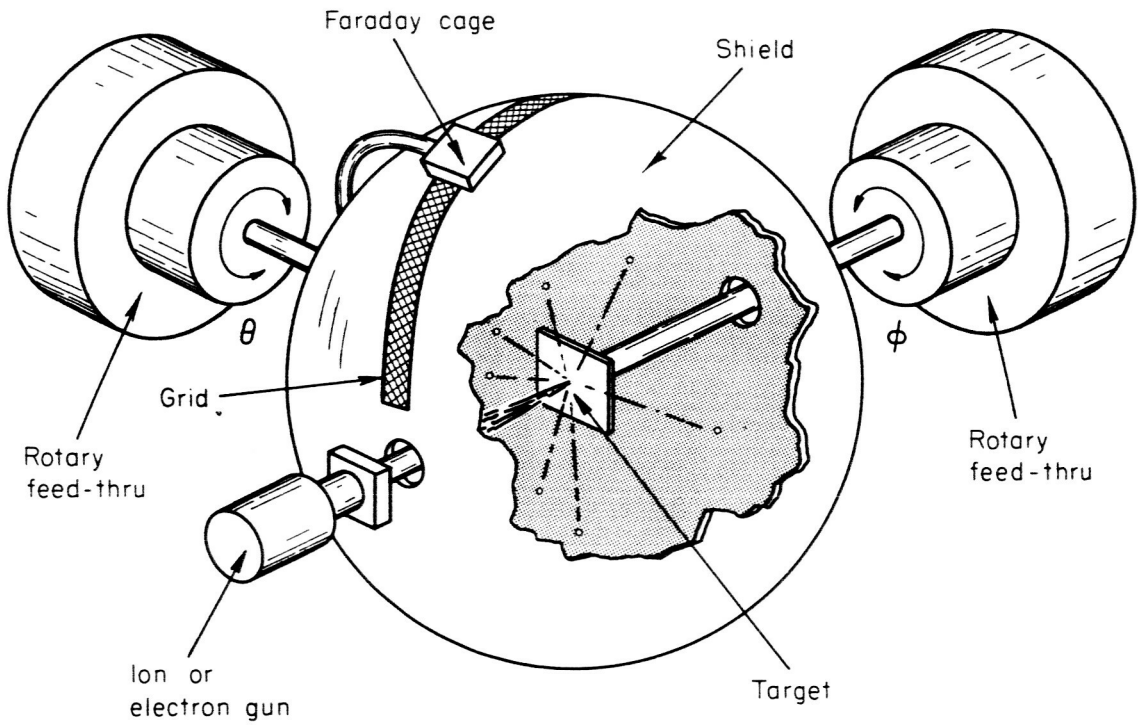
Faraday cage
Shield
θ
φ
Grid
Rotary
feed-thru
Rotary
feed-thru
Ion or
electron gun
Target

Fig. 2.3.

distribution of the ejected electrons. This is accomplished by modulating the ejected electron beam and using an A.C. detection technique similar to the one described in a previous progress report.[6]

The azimuthal angle, φ, is varied by rotating the target. The latitudinal angle, θ, is varied by rotating the collector. In the configuration shown in Fig. 2.3, interference between the ion gun and collector makes measurement of the distribution impossible for approximately 15^{o} of the latitudinal angle. If it is found that the angular distribution does not depend significantly on the angle of incidence of the ion beam, a second experimental configuration will be used. In this configuration the impinging ion or electron beam will be at an angle of about 15^{o} relative to a line normal to the target surface. With this arrangement, it will be possible to measure the ejected electron intensity over the entire 2π steradians.

In order to rotate the Faraday cage and tungsten target, an ultra-high vacuum rotary motion feed through, or vacuum crank, has been designed. Two such cranks are being constructed in the C.S.L. shop. A schematic of the crank is shown in Fig. 2.4.

The dotted line picture shows the position of the drive shaft and bushing assembly when the crank has been turned through 180^{o} relative to the solid line picture. The point A is fixed on the drive shaft and does not rotate relative to the vacuum system. The drive shaft is free to turn in the bushing assembly and drives the rotary output via a slot in the disk.

---

[6] March, April, May 1963 Progress Report, p. 16.

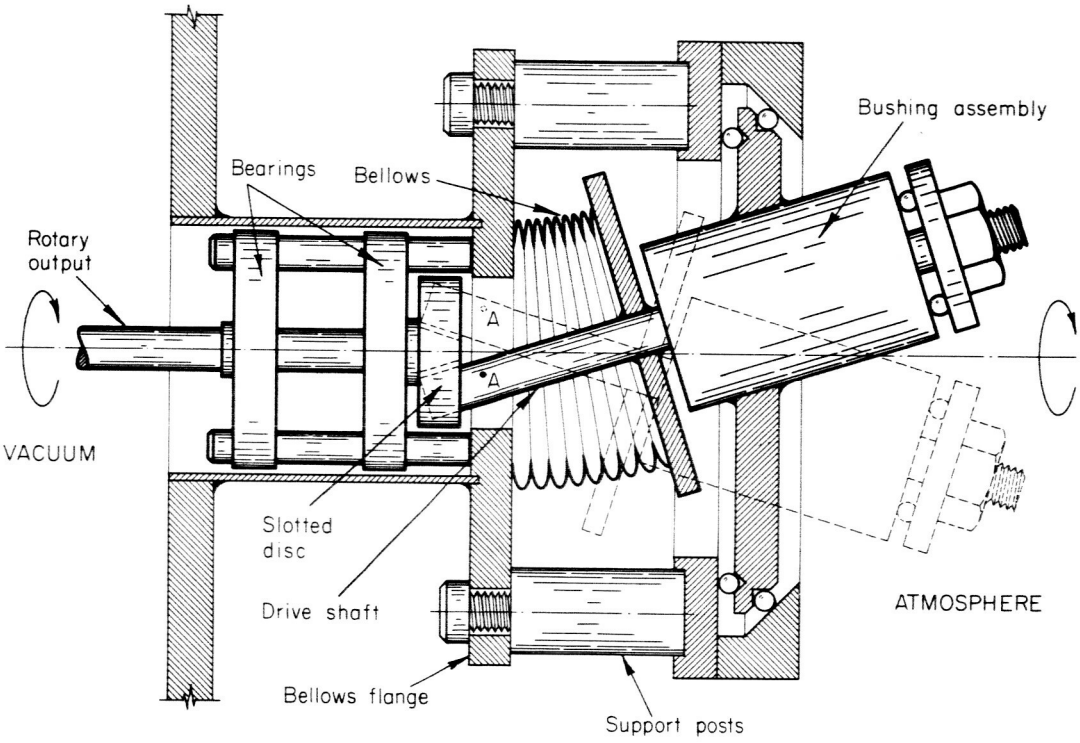
Bushing assembly
Bearings
Bellows
Rotary output
A
A
VACUUM
Slotted disc
Drive shaft
ATMOSPHERE
Bellows flange
Support posts

Fig. 2.4.

For bakeout the entire driving mechanism is slipped off by removing the bolts holding the support posts to the bellows flange and by removing the nut on the drive shaft. A clamp has been designed to keep the bellows from collapsing due to atmospheric pressure. The crank should allow accurate positioning of counter and target, easy angular calibration, smooth rotary motion, and long bellows life.

3. COMPUTER

R. M. Brown
S. Fenves
R. Jenks
L. Kypta
E. Manning
V. Metze
J. Stifle
R. Trogdon

3.1 Introduction

This division is concerned with the design and application of digital computers for information processing, primarily in the areas of real time and non-numerical operations. The present work lies in three areas: the development and supervision of the CSL computing facilities centering on the CSX-1 and a CDC 1604 computer, studies in artificial intelligence, and studies in methods and programs for time-shared use of digital machines.

3.2 CSX-1 Computer

3.2.1 Operations

Period: February 28, 1964, to June 3, 1964

Total running time	1987.8 hrs.
Ave. per day (7 day week)	20.9 hrs.
Operational Time: 99.84%	1984.64 hrs.
Scheduled Maintenance Time:	0.0 hrs.
Emergency Maintenance Time: 0.16%	3.16 hrs.

Breakdown of emergency maintenance time:

1.5 hrs: repair and adjust paper tape reader

1.5 hrs: locate and repair wiring error

.16 hrs: replace faulty indicator lamp

L. Hedges
J. Knoke

3.2.2 Modifications

The on-line flexowriter has been modified to permit operation on an interrupt basis if a programmer so desires.

Additional equipment has been designed and installed providing for more general communication between the CSX-1 and the 7094. A former PLATO keyset has been modified and installed as an input device from the cathode ray tube display. The keyset operates on an interrupt basis and can transmit any of 64 characters, including the standard typewriter symbols.

Three new instructions have been added to the CSX-1. These instructions allow simultaneous multiple program entry to and exit from subroutines.

J. Stifle

3.2.3 CSX-1 Display System

Early in the past quarter, a keyset was added to the display complex to further exploit the display unit currently operating in conjunction with the CSX-1. The system can now be regarded as a loop in which a man responds to the display by operating the keyset, which in turn causes the computer to change the display. It is possible to write programs for the CSX-1 such that the display will always show information easily recognizable by the man, and such that the keyset buttons can be labeled with familiar functions and symbols. It follows then that the loop can be one in which the man is ignorant of digital computers, programming, and related topics. As such, the loop has application in a wide variety of disciplines ranging from chemistry to mathematics and circuit design. Which discipline shall be operational

at any one time is wholly determined by the program residing in the CSX-1. From an operational point of view, the system is an extensive tool with which an operator can perform complicated and otherwise time-consuming functions within a given field of study.

As a typical example of what can be done with this loop, a program has been assembled to enable an operator to do a primitive form of function analysis. The functions referred to here are single-valued mathematical functions of the form $y = f(x)$. The program is capable of storing up to twenty different functions (over a range of x specified by the operator) in twenty psuedo-registers. With the keyset, the operator has the ability to execute arithmetic operations on any pair of functions thereby forming a new function. Originally, functions are assembled from constants and the variable x both of which can be inserted into any psuedo-register by manipulating the keyset. The operator can display the function contained in any one of the psuedo-registers upon demand via the keyset. All functions are displayed with labeled coordinate axes.

In its present form, the program is most useful in dealing with polynomials. Typically, it is possible to form and display complicated polynomials within three minutes. Once formed, such information as minima, maxima, roots, and poles can be read off the display with accuracies of 2% of full-scale.

Work in the near future will be directed at increasing the usefulness of the program. The list of keyset functions will be expanded to include "differentiate", "integrate", and "display

parametrically". In addition, the numbering system is to be changed, so that ultimate accuracies as high as 1 part in 10^{100} shall be available.

L. S. Kypta

3.3 CDC 1604 Computer: Operations

Period: February 28, 1964 to May 31, 1964

Total Running Time:	1077.00 hrs.
Ave. per day (7 day week)	11.46 hrs.
Operational Time: 94.27%	1015.25 hrs.
Preventive Maintenance Time: 5.59%	60.25 hrs.
Emergency Maintenance Time: 0.14%	1.5 hrs.

Breakdown of Emergency Maintenance Time:

1.00 hours: card failure in 1607 magnetic tape unit

0.50 hours: clear pushbutton for A register failed to operate, replaced with new button switch

L. Hedges
E. Neff

3.4 Artificial Intelligence: Game Playing Studies

The work utilizing the game, NIM^2, has been terminated. These studies have involved development of a set of calibrated "player" programs (i.e. programs which play with a fixed non-perfect level of performance) and experiments with a learning player whose performance can be accurately measured at any stage of development. Results are reported in CSL report, R-208.

E. Manning

3.5 Time Sharing Studies

3.5.1 The DIOG System

Programming is underway for the DIOG system for experimental time-sharing of an IBM 7094 computer via the CSX-1 computer. The general philosophy and structure of the system were described in the progress report of the previous quarter.

The main difficulties appear to lie in achieving the necessary changes to the current monitor system for the 7094 to permit the CSX-1 to interrupt the normal service background. Consequently, the first version of DIOG will be run without interrupt feature, but rather as a conventional 7094 program to permit checkout of the operational communications.

R. M. Brown
R. D. Jenks
S. Fenves

3.5.2 Experimental Measurements on the SMP-CSX-1 System

The previous quarterly progress report described the system set up and now operating for on-line control of bubble chamber data processing in cooperation with the High Energy Physics Group of the Physics department. This system represents a rather carefully organized man-machine combination, wherein the respective roles are well matched to the capabilities of the two components. Inasmuch as very little experimental data is available concerning the actual parameters of such programs, a set of experimental runs were made to determine the following parameters: (1) the percentage of time actually required for execution of the program, and (2) the spectrum of times during

which the computer is awaiting a human response. Detailed results will be reported in a paper.

The technique for making these measurements, itself, is of interest in as much as the SMP Program had to be enveloped in a monitoring program which sampled the performance at different time intervals. For this purpose, the multiple interrupt levels of the CSX-1 proved invaluable; a total of six different levels were operable at varying times in the experimental runs.

R. M. Brown

4. SYSTEMS

Circ. & Commun.	Control Systems	Switch. Systems
M. E. Van Valkenburg	J. B. Cruz, Jr.	S. Seshu
J. K. Aggarwal	S. D. Agashe	H. M. Barnard
R. B. Ash	D. Gieseking	K. E. Batcher
D. H. Cooper	T. E. Mueller	W. K. Chen
P. Ponzo	T. Murata	A. Dervisoglu
R. A. Rohrer	W. R. Perkins	G. Dodd
N. Wax	R. A. Rohrer	B. Elliott
	D. Snyder	W. Mayeda
	M. Sobral, Jr.	K. Onaga
	G. Tahim	A. Paul
	R. Werner	D. Rain
		J. A. Resh

4.1 Self-Diagnosis

The programs for organizing a sequential circuit and for generating a test procedure for a given sequential circuit have been completed. Two reports on these programs are currently in the process of being issued.

Mr. Eric Manning and Mr. Szu-Chi Chang are expected to join the group on self-diagnosis in June 1964. It is hoped that the work of organizing the CSX-1 computer for purposes of self-diagnosis can now proceed fairly rapidly.

S. Seshu

4.2 RLC Network

Properties of the A-matrix of RLC half-degenerate networks have been studied.

The conditions for the realizability of a given matrix as the A-matrix of a half-degenerate RLC network have been reduced to the realizability of a resistive network.

Ahmet Dervisoglu

4.3 NOR Network Study

A necessary and sufficient condition for the realizability of a flow table by a speed-independent NOR network has been found. This, together with other results, is presented in CSL Report R-205, May, 1964. This report is identical to a Ph.D thesis in Electrical Engineering June, 1964.

K. E. Batcher

4.4 Quasi-Linear Sequential Machines

A necessary and sufficient condition has been found for the state diagram of a completely specified sequential machine, with a given encoding of states, to be realizable as a quasi-linear sequential machine. Also obtained is a canonical realization which provides a means to realize any state diagram as an incompletely specified quasi-linear sequential machine. A report on these results is under preparation.

H. Y. Chang

4.5 Universal Compiler

Recent work on the universal compiler has been directed towards the construction of a compiling process P and an associated source language L. Once the pair (L,P) has been obtained, it is to form the basis of compilers for a number of different computers. The fundamental requirement is that the task of producing a compiler $C_M(L,P)$ for any particular machine M should demand only a small amount of creative programming effort.

The result to date is the rough outline of a process P with a machine-independent description which

(1) promises to admit an associated L within which P itself can be programmed, while otherwise imposing only modest constraints on L;

(2) seems to be flexible enough to allow the recognition of special characteristics which a given object machine may have, so that these can be used to obtain efficient compiled programs.

If our scheme can be completed in detail, then it will be possible to write an L-program $C_L(L,P)$ which, when translated as a machine-language program $C_{M_o}(L,P)$ for some machine M_o will be a compiler which can accept as data

(i) a specification of certain salient features of some object machine M (e.g. the number of different types of registers, the number and word-length of each type, etc.);

(ii) a description of M-language (in the form of a number of M-language strings for each L-statement, associated conditions for equivalence, selection criteria, etc.);

(iii) an L-program.

The output of $C_{M_o}(L,P)$ will then be a translation into M-language of the input L-program. Thus we can obtain the desired compiler $C_M(L,P)$ by using $C_L(L,P)$ as the input L-program. When $C_M(L,P)$ is in actual use as a compiler for machine M, of course, the results of reading parts (i) and (ii) of the data could be saved as part of the systems tape and this portion of the compiling operation would be bypassed in the subsequent use.

J. A. Resh
W. Mayeda

4.6 Lossy Communication Nets

The study of a lossy communication nets has been completed. We found that there exists a saturated cut set when the maximum flow is sent from a vertex i to a vertex j in the net. There is a relationship among terminal capacities which is similar to a triangular reltionship in lossless communication nets as follows. Suppose $\bar{t}_{pq}$ is the maximum flow which is sent from vertex p in order to receive maximum flow at vertex q. Also suppose $\underline{t}_{pq}$ is the maximum flow which can be received at vertex g when the maximum flow is sent from p. Then $\underline{t}_{ij}$, $\bar{t}_{ij}$, $\bar{t}_{ik}$ and $\underline{t}_{kj}$ (when i, j and k are any vertices in a net) must satisfy either $\underline{t}_{ij} > \underline{t}_{kj}$ or $\bar{t}_{ij} \geq \bar{t}_{ik}$. This part of the results in Report R-200 has been accepted as a paper for the International Conference on Microwaves, Circuit Theory, and Information Theory in Japan.

The properties of classes of paths where each class consists of all possible paths between a pair of vertices in a non-separable graph have been studied. It is clear that such properties will help a great deal when one synthesized S.C. switching network which satisfies a set of given switching functions. Also by the use of generalized classes of paths, we can find all possible trees in a linear graph. The details are shown in Report R-212.

Suppose we defin a linear graph as $\{G,V\}_f$ where G is a set of edges, V is a set of vertices and f is a 1-1 mapping function which maps each edge e in G to a pair $(\zeta_1\zeta_2)$ in VxV. ζ_1 and ζ_2 are known as the two endpoints of edge e. By this definition, we can define operation Θ on linear graphs as

$$\{G_1,V_1\}_f \ \Theta \ \{G_2,V_2\}_f = \{G_1 \Theta\ G_2,\ (V_1 \Theta\ V_2) \cup \Omega(G_1 \Theta\ G_2)\}$$

where $\Omega(G)$ is the set of vertices each of which is an endpoint of at least one edge in $G_1 \Theta\ G_2$. Operation Θ can be union, intersection, ring sum, etc. The use of these definitions will simplify and clarify the problems in linear graphs (Report R-203).

W. Mayeda

4.7 Switching Synthesis

The study of the synthesis of switching networks was continued. Synthesis by construction of a directed graph corresponding to a network satisfying a given switching function is being studied. This approach does not restrict the network to two-level logic as most current synthesis procedures do. Minimization of the number of network components is also being considered.

A. Paul

4.8 Expectation of Terminal Capacity of Probabilistic Nets

In the previous report,[1] the following problem was considered: Suppose the branch capacities of a subset of the edge set of the net be replaced by their individual expectations, that is, x to be replaced by $E\{x\}$ where x is branch capacity random variable, and when

$$E\{x\} = \Sigma\ \zeta_i\ \rho\{x = \zeta_i\},$$

and suppose these branches be non-probabilistic. If $\bar{t}_{ij}$ is expectation of the terminal capacity between vertex i and j of the original net and $\hat{t}_{ij}$ is a corresponding one of the derived net mentioned above, what is the relation between these two values? We conjectured

$$\hat{t}_{ij} \geq \bar{t}_{ij}.$$

[1] Progress report for Dec. 1963, Jan., Feb., 1964. Coordinated Science Laboratory, University of Illinois, Urbana, Illinois.

A mathematical proof of validity of the conjecture is given as follows: the terminal capacity t_{ij} is a function of random variables $x_1, x_2, \ldots, x_n$ where x_r represents capacity of r-th branch and takes discrete, non-negative values $\xi_{r1}, \xi_{r2}, \ldots, \xi_{rs_r}$ for each r,

$$t_{ij} = \varphi_{ij}(x_1, x_2, \ldots, x_n).$$

The expectation $\bar{t}_{ij} = E\{t_{ij}\}$ is given as

$$\bar{t}_{ij} = \Sigma\, \varphi_{ij}(\xi_{1k_1}, \xi_{2k_2}, \ldots, \xi_{nk_n})\; p(\xi_{1k_1}, \xi_{2k_2}, \ldots, \xi_{nk_n}),$$

where the sum is to range over all possible states.

According to the fundamental theorem of maximal flow, t_{ij} is equal to the minimal of the values of the cut sets separating vertex i and j. It is easily seen that φ_{ij} is concave with respect to each variable. For, if x_r increases from zero with the rest fixed, either one of the following takes place: (a) t_{ij} increases linearly while r-th branch is in a minimal cut set and remains constant after r-th branch is no longer in a minimal cut set as a result of an increase in r-th branch capacity; (b) t_{ij} remains constant from the start.

Jensen's inequality for a concave function φ of a single variable x states that

$$E\{\varphi(x)\} \leq \varphi(E\{x\}),$$

where E means the operation of expectation. If φ is concave there is a real number λ such that a line $\lambda(x-m) + \varphi(m)$ is greater or equal to $\varphi(x)$:

$$\varphi(x) \leq \lambda(x-m) + \varphi(m),$$

for all x. By taking expectation and letting $m = E\{x\}$, we have

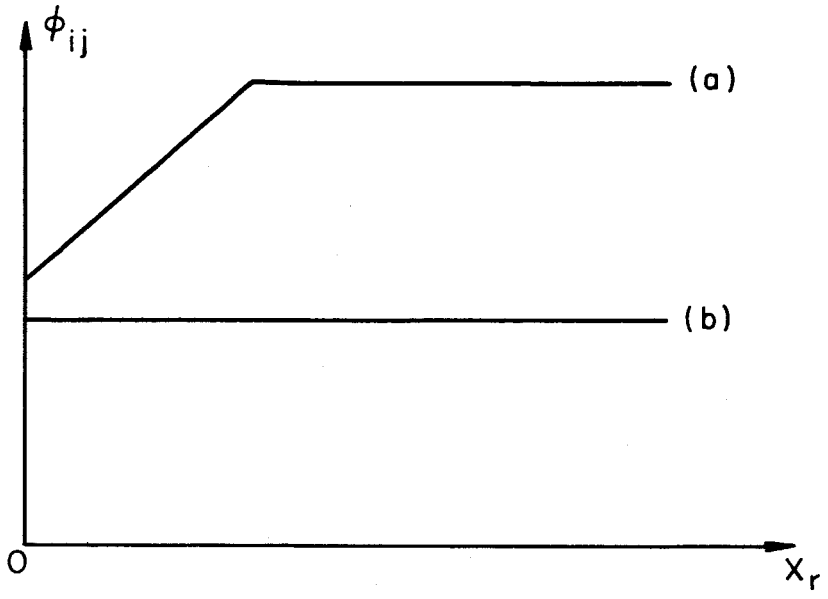

Fig. 4.1. Concavity of φ_{ij} with respect to each variable.

$$E\{\varphi(x)\} \leq \lambda(E\{x\} - m) + \varphi(m),$$

$$E\{\varphi(x)\} \leq \varphi(E\{x\}).$$

Jensen's inequality is readily extended to a function of independent random variables $x_1, x_2, \ldots, x_n$ with concavity for each variable by utilizing theorems on conditional expectations[2]. Jensen's inequality holds also for conditional expectations $E\{\ |x_1, x_2, \ldots, \hat{x}_k, \ldots, x_n\}$ where $x_1, x_2, \ldots, \hat{x}_k, \ldots, x_n$ means that x_k is missing from the set $x_1, x_2, \ldots, x_n$, that is

$$E\{\varphi(x_1, x_2, \ldots, x_n) | x_1, x_2, \ldots, \hat{x}_k \ldots, x_n\} \leq$$

$$\varphi(x_1, x_2, \ldots, E\{x_k\}, \ldots x_n).$$

Taking the expectation of the above inequality,

$$E\{E\{\varphi(x_1, x_2, \ldots, x_n) \ |x_1, x_2, \hat{x}_k \ldots x_n\}\} \leq$$

$$E\{\varphi(x_1, x_2, \ldots E\{x_k\}, \ldots, x_n)\},$$

the left side expectation is equal to $E\{\varphi(x_1, x_2, \ldots, x_n)\}$, so that we have

$$E\{\varphi(x_1, x_2, \ldots, x_n)\} \leq E\{\varphi(x_1, x_2, \ldots E\{x_k\}, \ldots x_n)\}.$$

If we apply a similar method to $\varphi(x_1, x_2, \ldots, E\{x_k\}, \ldots x_n)$ by taking conditional expectation $E\{\ | \ x_1, x_2, \ldots \hat{x}_k \ldots \hat{x}_\ell \ldots x_n\}$, $\ell \neq k$, expectation E successively, we get

$$E\{\varphi(x_1, x_2, \ldots, E\{x_k\}, \ldots x_n)\} \leq$$

$$E\{\varphi(x_1, x_2, \ldots E\{x_k\}, \ldots E\{x_\ell\}, \ldots x_n)\}.$$

---

[2] On the properties of conditional expectations, confer lecture note for Math. 452. University of Illinois, by J. L. Doob and also Stochastic Processes, John Wiley, 1953, by the same author.

Repeating the procedure we get a series of inequalities as summarized in the theorem we now quote.

Theorem: Let φ be a function of independent random variables $x_1, x_2, \ldots, x_n$ and concave with respect to each variable. Extended Jensen's inequalities hold as follows:

$$E\{\varphi(x_1, x_2, \ldots, x_n)\} \leq E\{\varphi(E\{x_1\}, x_2, \ldots, x_n)\} \leq$$

$$E\{\varphi(E\{x_1\}, E\{x_2\}, x_3, \ldots, x_n)\} \leq \ldots \leq$$

$$\varphi(E\{x_1\}, E\{x_2\}, \ldots E\{x_n\}).$$

In terms of terminal capacity, interpretation of the theorem is as follows: let G_o be the original net, and let G_r be a derived net by replacing branch capacities $x_1, x_2, \ldots x_r$ which are independent random variables with their individual expectations $E\{x_1\}, E\{x_2\}, \ldots E\{x_r\}$, respectively, and by regarding these branches as non-probabilistic. If we denote $\bar{t}_{ij}(G_r)$ $r = 0, 1, 2, \ldots, n$ as expectation of the terminal capacity between vertex i and j of net G_r, then

$$\bar{t}_{ij}(G_0) \leq \bar{t}_{ij}(G_1) \leq \ldots \leq \bar{t}_{ij}(G_n),$$

where n is number of the edges of the original net G_o. This completes the proof.

Kenji Onaga

4.9 Probabilistic Communication Net Synthesis

The work reported in Section 4.13 of the last progress report has been completed. A synthesis procedure to realize an expected value terminal capacity matrix as a net with a tree structure is given in CSL Report R-209.

H. M. Barnard

4.10 Graph Theory

A unistor, as defined by Mason[3], is an oriented edge in which flow is a function of the wright of the edge's initial vector and a function of the edge weight. Work has continued this quarter on developing techniques which utilize the unistor in the solution of linear systems, active networks, and the analysis of communication nets.

G. Dodd

4.11 Parameter Variations in Control Systems

Our new formulation of the parameter variation problem[4,5] has been extended to linear, time-varying, multi-input, multi-output systems. Direct comparison of the errors due to parameter variations in open-loop and closed-loop systems leads to a sensitivity operator S,

$$\underline{e}_c(t) = S\, \underline{e}_o(t). \tag{1}$$

We have shown that a necessary and sufficient condition for the closed-loop system to be better than the open-loop system in the sense of

$$\|\underline{e}_c(t)\| \leq a\, \|\underline{e}_o(t)\|,\ a < 1, \tag{2}$$

is

$$\|S\| < 1 \tag{3}$$

Moreover, we have shown that (2) is equivalent to requiring the operator S to be a contraction. Useful forms of these conditions

---

[3] Mason, S. J., "Topological Analysis of Linear Nonreciprocal Networks," Proc. IRE, vol. 45, pp. 829-838; June 1957.

[4] J. B. Cruz, Jr., and W. R. Perkins, "A New Approach to the Sensitivity Problem in Multivariable Feedback System Design," IEEE Trans. on Automatic Control, vol. AC-9; July 1964.

[5] W. R. Perkins and J. B. Cruz, Jr., "The Parameter Variation Problem in State Feedback Control Systems," 1964 Joint Automatic Control Conference, Stanford, California; June 1964.

have been obtained for specific norms.

J. B. Cruz, Jr.
W. R. Perkins

4.12 Optimal Control of Cooperative Systems--The Rendezvous Problem

The rendezvous problem is defined as follows:

Given two dynamic, controlled systems

$$\dot{\underset{\sim}{x}} = A\underset{\sim}{x} + B\underset{\sim}{u},$$

$$\dot{\underset{\sim}{y}} = C\underset{\sim}{y} + D\underset{\sim}{v},$$

find the control signals $\underset{\sim}{u}$ and $\underset{\sim}{v}$ such that $x_i(T) = y_i(T)$ $i = 1, 2, \ldots, k < m < n$, where m and n are the orders of the two systems respectively, for some $T > t_o$ and such that the performance index

$$J = \frac{1}{2}\int_{t_o}^{T} (\underset{\sim}{\ell}^t Q\underset{\sim}{\ell} + \underset{\sim}{u}^t D_1\underset{\sim}{u} + \underset{\sim}{v}^t D_2\underset{\sim}{v})\, dt,$$

where $\ell_i = x_i - y_i$ for $i = 1, 2, \ldots, k$, is minimum. By defining the rendezvous problem in this manner, the problem in which one control signals is known a priori or one system is uncontrolled is eliminated. This general problem can be solved, yielding an open-loop control law, by Pontryagin's Maximum Principle.

An optimal feedback control law has been found using the calculus of variations if the plant is single-input, linear, time-invariant, completely controllable.

Due to the increased usage of digital controllers, the discrete problem was also formulated and solved. The statement of the problem is given by direct analogy to the continuous problem. The systems are described by

$$\underset{\sim}{x}(k + 1) = A\,\underset{\sim}{x}(k) + B\,\underset{\sim}{u}(k)$$

$$\underset{\sim}{y}(k+1) = C\,\underset{\sim}{y}(k) + D\,\underset{\sim}{v}(k)$$

The rendezvous conditions are the same and the performance index beomes

$$J = \sum_{k=0}^{T} \underset{\sim}{x}(k)^t\, Q\, \underset{\sim}{x}(k) + \underset{\sim}{u}(k)^t\, D_1\, \underset{\sim}{u}(k) + \underset{\sim}{v}(k)^t\, D_2\, \underset{\sim}{v}(k)$$

where T is the rendezvous time.

D. Gieseking

4.13 Limit Cycles in Discrete-Time Systems

The purpose of this research is to find computationally simple tests for finding limit cycles in unforced discrete-time control systems having piecewise-linearities. Two methods have been developed for determining the trajectory in state space for sampled-data systems with a single nonlinearity, a single sampled-and-hold element, and a linear dynamic transfer function of any order. These methods can be used also to determine the stability of the limit cycles. Stability of sampled-data systems having a relay with a dead zone or with hysterisis has been considered thoroughly.

An extension of one of the methods for finding limit cycles in sampled-data systems gives a method of finding limit cycles in a system with a single nonlinearity and a multiple-order sample-and-hold element.

The objective of future research will be to extend the above methods to a larger class of discrete control systems.

R. Werner

4.14 Control Systems

In addition to the completion of the work on singular solutions of optimal control and linear switching, a new project has been

undertaken. A meaningful measure of the sensitivity of an optimal system has been formulated and related to various design criteria. This work will appear shortly as CSL Report R-213.

R. A. Rohrer
M. Sobral, Jr.

4.15 Time-Lag Systems

Gradient techniques are being developed for the solution of an optimum control problem involving a plant with time delay and a fixed controller which operates only on the present state of the plant.

T. E. Mueller

4.16 Stochastic Optimal Control

Investigations have been initiated on certain properties of functionals associated with systems subject to random disturbances. The relationship of these properties to aspects of optimal control theory is being studied.

Limited results have been achieved for examples chosen from both discrete and continuous systems. Numerical data is being obtained for a continuous, first-order, fixed time of control example.

M. K. Sain

4.17 Numerical Optimization and its Application

An earlier technical report[6] indicated that some system design problems could be treated by turning them into optimization problems and introduced ideas of the "direct design" and the "optimum

[6] T. Murata, "The Use of Adaptive Constrained Descent in Systems Design," CSL Report R-189; December, 1963.

design" through examples in filter and equalizer designs. Further applications of the direct search method are being investigated in order to develop or improve a numerical optimization technique. For example, arbitrary gain equalization is attempted using the direct design scheme and fairly irregular curves can be realized. However, as the number of system parameters increases, more difficulties arise in finding the true minimum.

T. Murata

4.18 Optimal Control Subject to Sensitivity Considerations

The problem of determining the optimal control when there is some uncertainty in the plant parameters is being studied. In this problem, it is assumed that the differential equations describing the system are known except for certain parameters which are only partially, perhaps statistically known. The original performance index must then be modified to reflect this imperfect knowledge, and the control signal can then be optimized for this modified performance index. Various modifications of the performance index and the accompanying computational problems of solution are being investigated.

T. J. Killian

4.19 Time Optimal Control of Nonlinear Sampled-Data Systems

The control system is given by the linear differential equation

$$\dot{\underset{\sim}{x}}(t) = a(t)\, \underset{\sim}{x}(t) + \underset{\sim}{b}\, f_m(t),$$

with $\underset{\sim}{x}(0^+)$ given. The constraints on the control signals are

1. $f_m(t) = f_m$ (constant), for $(m-1)\,T < t < mT$ where T is the sampling period;

2. $|f_m| \leq 1.0$, for m=1,2,3,...

The performances of the control system are

1. $\underset{\sim}{x}_d = \underset{\sim}{x}(NT)$, where $\underset{\sim}{x}_d$ is the desired state and N is a finite number;

2. N is a minimum number.

First, the problem is to investigate whether there exists a finite number N such that

$$\underset{\sim}{x}_d = \underset{\sim}{x}(NT)$$

Second, the problem is to find an optimal strategy corresponding to a minimum number N from all the possible N satisfying the above equation.

Necessary and sufficient conditions for complete controllability, attainability, and reachability of single-input, time-invariant, sampled-data systems are given. Conditional controllability, attainability and reachability are introduced and sufficient conditions are derived. Complete controllability and attainability of single-input, time-varying, sampled-data systems are investigated also. Simple sufficient conditions are derived when the system matrices are either asymptotic to constant matrices or periodic. Procedures for the formulation of optimal strategies are discussed. The optimal strategy used in this research involves forcing the system to the boundary surfaces first, and then to the desired state. Detailed results are given in Technical Report R-210.

S. M. Win

4.20 Nonlinear Differential Equations

The system of differential equations

$$\dot{x} = P(x) + Q(y) + p(t)$$

$$\dot{y} = R(x) + S(y) + q(t)$$

has been studied, where P, Q, R, S, are polynomials and the functions p(t) and q(t) are periodic functions of time.

The nature of the singularities of the system has been investigated, and confining regions constructed which bound periodic solutions when they exist.

A report on this work is being prepared.

The manuscript of a report, to be submitted as a paper, has been completed. The manuscript, entitled "On Certain Relaxation Oscillations: Confining Regions", gives an explicit method for constructing an annular region which contains a periodic solution of the generalized Liénard equation

$$\ddot{x} + \mu f(x)\dot{x} + g(x) = 0.$$

The van der Pol equation is a special case.

Another report, entitled "On Certain Relaxation Oscillations: Asymptotic Solutions", describing analytic methods when $\mu \gg 1$, is in preparation.

J. K. Aggarwal
P. J. Ponzo
N. Wax

4.21 Circuit Theory

Three of the circuitry theory projects reported in the previous progress report have been completed and will appear shortly: Mr. B. S. Kipnis has evolved a simple relation between gain and stability of linear active two-port networks; Mr. R. A. Hoyt has found a general synthesis procedure for distributed networks; Mr. J. P. Herner

has solved the matching problem for nonlinear, time-invariant networks. Work continues on the remaining projects.

R. A. Rohrer

4.22 RC Synthesis Investigation

The conditions which must be satisfied in this synthesis procedure have been simplified so that only two tests are now necessary. The procedure is now being programmed in order to run numerical examples on the CDC 1604 computer.

Bruce D. Elliott

5. PLATO

D. Bitzer
R. A. Avner*
R. Blomme
E. DeWan
J. Easley*
H. Gelder*
W. Golden*
E. R. Lyman
L. Morgan
M. Secrest
S. Singer
R. Suchman*
B. W. Voth
R. Willson

5.1 Introduction

The purpose of the PLATO project is to develop an automatic teaching system for tutoring simultaneously a large number of students in a variety of subjects. The central control element of the teaching system is a general purpose digital computer. The PLATO system differs from most teaching systems in that a single high speed digital computer is used to control all student stations. Thus, it can bring to bear the power of a large digital computer in teaching each student.

5.2 PLATO III Programming

The first real use of the CATORES program (general PLATO III master program for any PLATO teaching logic) was made by the Scientific Inquiry project of Dr. Richard Suchman. The program, REPLAB, was completed this spring and thirty-eight students successfully took the lesson. The student runs uncovered several small problems in CATORES and in the special subroutines written for REPLAB. These problems were easily soluble so the student use could continue, but as a result several CATORES improvements have suggested themselves which will be undertaken this summer. Some of these are on-line parameter input, restarting lessons at previous stopping points, improved doping routines, etc.

---

*CSL Consultants

The mathematical problem-solving program, the new PROOF, has many subroutines now ready for codechecking with the PLATO compiler.

Programming is underway to demonstrate the use of two entirely different lesson sequences simultaneously, one at one student station, one at another.

E. R. Lyman
M. Secrest
J. Easley

5.3 Inquiry Training (REPLAB)

REPLAB gives promise of being a tool for the multi-dimensional analysis of the inquiry process. As the subject operates this computer-controlled responsive environment, he is registering his patterns of inquiry and providing data that characterize his own particular patterns as an inquirer and as a thinker in general.

Preliminary analysis of the data on 27 sixth grade subjects shows relationships between REPLAB variables that can be classed as cognitive style or mode of attack.

For the present, the most significant discrimination that can be made through the REPLAB analysis is between children who deal with their world more or less intuitively and in large global hunks and those who deal with it analytically in small segments. Several REPLAB variables seem to reflect how analytical the child is. For example, the number of times the subject reviews the problem film is negatively correlated with five outside test scores all of which reflect cognitive control. The two highest positive correlations are with measures that reflect looseness and fluency in cognitive performance.

Another example of a REPLAB variable that discriminates the tight focussed and analytical inquirer from the loose, diffuse and non-analytical one is the frequency of property verification. This score is positively correlated with the outside measures of cognitive control and negatively correlated with the outside measures that reflect non-analytical thinking.

A factor analysis is presently being performed on 17 REPLAB variables and 37 outside variables to determine just what factors are present and how the REPLAB variables are able to identify these factors in the inquiry behavior of children.

R. Suchman

5.4 Instruction in PLATO Lesson Preparation

Work continues on the series of lessons to teach non-technical persons the operation of the PLATO system. The logic associated with the lessons has been outlined and is ready to be coded in PLATO compiler language. The former program, Perimeter of Polygons, used to demonstrate the tutorial logic is being updated and augmented to illustrate the wider range of flexibility in the PLATO III system. The latter program is to be used in conjunction with the new lesson-preparation sequence to instruct potential lesson writers.

L. Morgan

5.5 PLATO III System Equipment

During this quarter work continued in the development and construction of circuitry required for the realization of a 20 student station teaching system.

Circuitry constructed to date includes all circuitry required to operate only two student stations. The remaining circuitry required for the operation of additional student stations is undergoing packaging.

Development continues on special circuitry which will update present circuitry or provide special system facilities. Included in this circuitry is transistor deflection, power control, master keyset, and master video switch circuitry.

B. Voth

5.6 Plasma Discharge Display Tube

The purpose of the plasma discharge display tube is to develop a less expensive replacement for the present storage tube system. Work during this quarter has been directed towards the problem of races and firing of adjacencies within the array.

R. H. Willson

6. VACUUM INSTRUMENTATION

D. Alpert L. Simonelli W. Schuemann F. Steinrisser

6.1 Surface Impact Ionization

As was reported in the previous progress report, a tube has been designed and built for a series of experiments on the interaction of slow electrons with adsorbed layers of gas on metal surfaces. These experiments are the continuation of a study which has been in progress for over a year now. Previous progress reports, especially June-August, 1963, describe the earlier work. These interactions have been shown to be responsible for anomalous pressure readings in ionization type vacuum gauges. They may also give rise to anomalous effects in other devices where electrons are incident on surfaces. Apparently both ions and neutrals can be emitted from a surface as the result of the interaction.

Although the cleaning action of electron bombardment on a metal surface, due to the removal of atoms and molecules, is well known, very few investigations have been made on the mechanism which is responsible for the release of material from the surface. Independently we at CSL and Redhead have observed the formation of positive ions by electron bombardment in an ionization gauge. Moore has extensively studied the system Mo-Co and Redhead the system Mo-O. Young has studied the effects of electron bombardment of oxide films (Cu, Ni, Mo, Te, Ti). We have not been able to reproduce Young's results on Mo, however.

The purpose of our experiment is to obtain more data on the surface impact ionization in order to determine how the gas is bound to

the surface. In order to do this we are studying the maximum efficiency of ion production, the threshold value for the ion production, and the relationship of sample temperature to ion production for Mo, Pt, and Cu. The tube we are using in these experiments is similar to the one used by Redhead in his studies of this effect, except that we have lowered the voltage between the filament and the first grid to 1.5 volts, to prevent any oscillation from modifying the electron energy. Also, a shield has been placed between the filament and sample to prevent material evaporated from the filament from reaching the sample. The biggest problem encountered in putting the tube into operation was finding a filament which would provide an essentially mono-energetic source of electrons. This problem was solved by using a very short tungsten hairpin filament where the voltage across the emitting portion is probably less than 0.25 volts. This tube is shown schematically in Fig. 6.1.

We have admitted oxygen into the vacuum system with a molybdenum sample in the tube. We measured a threshold for impact ionization on molybdenum of 17.5 $\pm$ .2 volts (uncorrected for contact potential). This compares with Redhead's value of 17.6 $\pm$ .2 (corrected for contact potential).

The percentage of ions produced which are collected has not yet been calculated, but it will be close to 0.5. This figure gives us 10^{-5} ions/incident electron and is very close to Redhead's value. The curve of surface ion current as a function of electron energy is shown in Fig. 6.2.

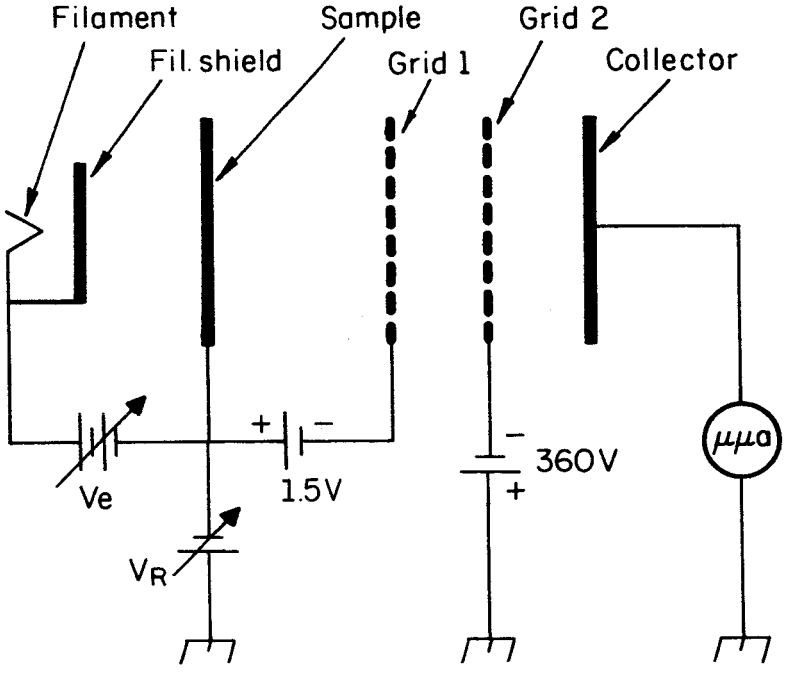

Fig. 6.1. Schematic of Impact Ionization tube.

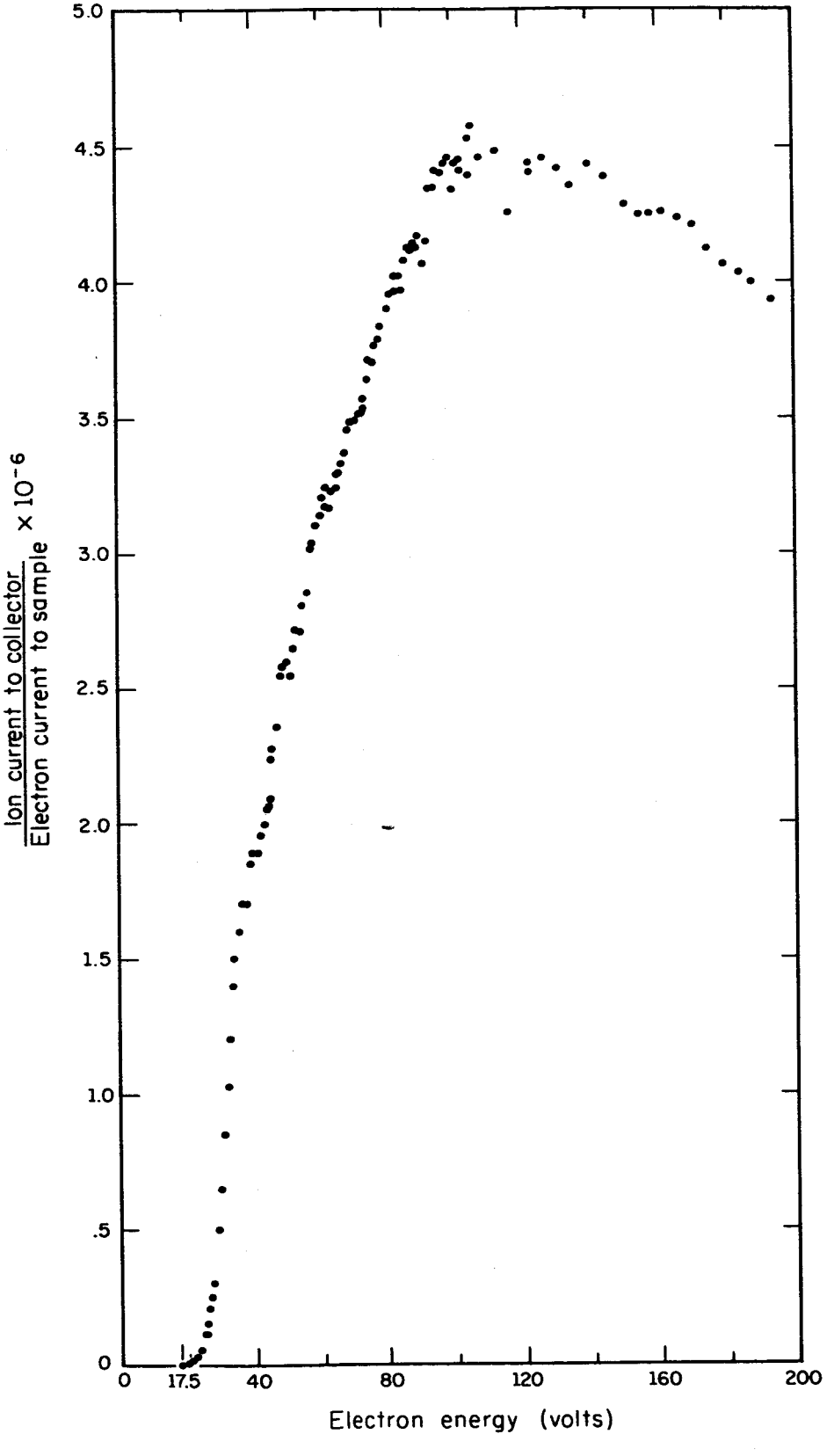

Fig. 6.2. Curve of Ion Current to the Collector versus Impacting Electron Energy.

The energy distribution of the ions has been measured. These results are in Fig. 6.3. The maximum occurs at a value somewhat between the values Redhead gave for O_2 and CO.

The values quoted above vary considerably, depending on experimental technique, and further experiments are necessary to determine what the important parameters are.

When O_2 was admitted with the sample hot ($\approx 700^{\circ}C$), an oxide was presumably formed on the molybdenum. We found no ion production from oxidized molybdenum. This is contrary to the results of Young. On the other hand if the O_2 was admitted with the sample at room temperature, and the ion production checked as a function of increasing temperature, the ion production would remain constant, and at approximately $1000^{\circ}C$ there would be a burst of gas in the system, and the ion production would disappear.

The next step in the experiment is to introduce CO alone and try to determine in this way what the contribution of CO is. Then we will move on to platinum.

6.2 Lanthanum Boride Filaments

This quarter, a technique for electrophoretic deposition of LaB_6 was developed. Although the conditions are not critical, the best results have been obtained by placing 3 gms of LaB_6 in 90 cc. of ethyl alcohol along with 10 cc. of a solution consisting of distilled water and 2 milligrams of $LaNO_3$. The deposition is done at room temperature with an anode to cathode voltage of 50 volts and the anode to cathode spacing set at 5 cm. The filament to be covered is the cathode.

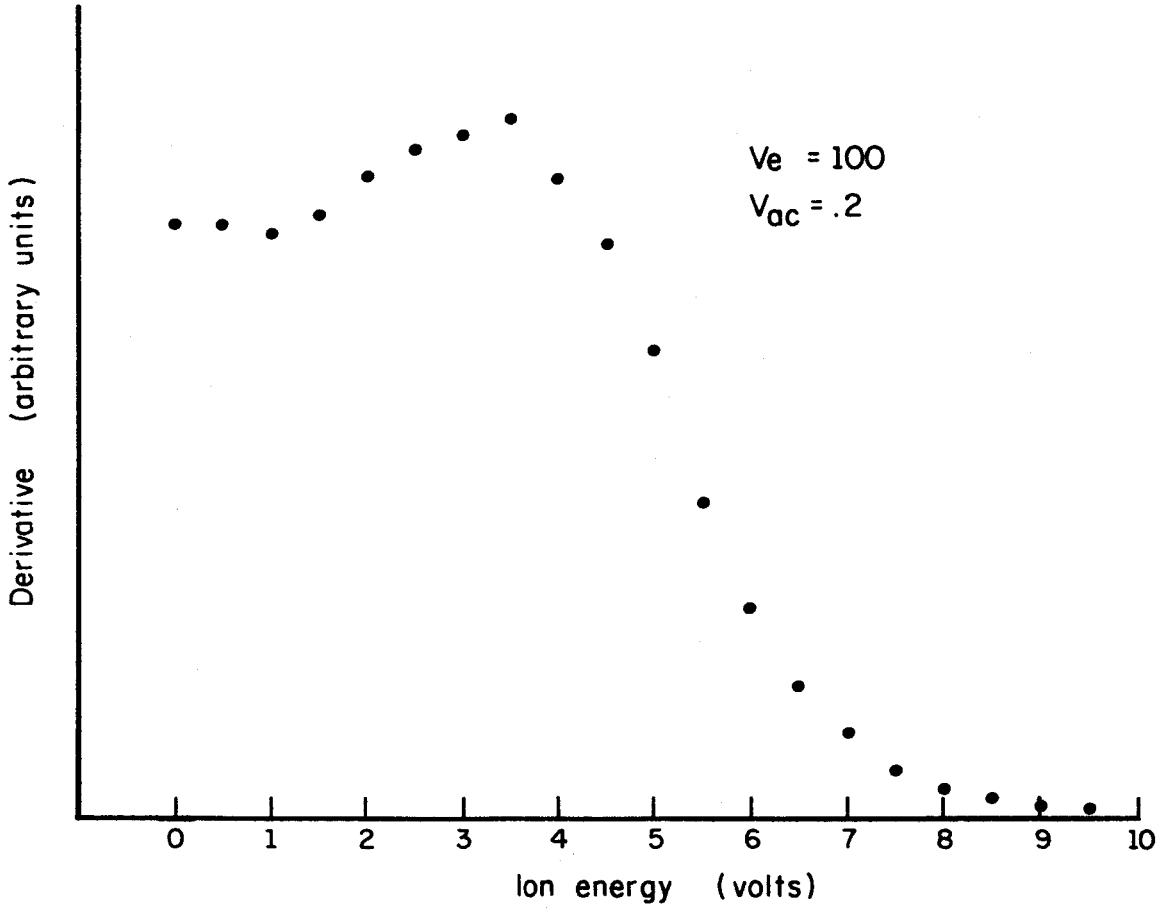

Fig. 6.3. Ion Energy Distribution (Uncorrected) versus Ion Initial Energy.

We have obtained good adherence to W, Mo, Ta, Ni, and Re. The adherence to the surface is improved if the metal is previously electropolished.

Of the metals tried only Rhenium gave a stable emission current. We have obtained currents of 5×10^{-2} amperes/cm^2 at 1370^{o}C with no apparent deterioration of the filament over the period of one month.

6.3 Photocurrent Suppressor Gauge

The photocurrent suppressor gauge performance at lower pressures has been improved as the result of a change in the suppressor ring geometry. Fig. 6.4 shows the increased size of the suppressor electrode. The increased size permits the suppressor to be run at lower voltages. At any given pressure, the suppressor voltage required is 1/4 of its previous value.

In the past quarter the photocurrent suppressor gauge has read currents corresponding to 1×10^{-12} torr with the suppressor voltage set at 200 volts. Fig. 6.5 compares the old and new suppressor voltage versus collector current curves.

A troublesome behavior which has been observed many times is an oscillation in an ionization gauge giving rise to negative collector currents. The suppressor gauge has the unusual characteristic that the oscillation becomes more intense as the suppressor voltage is made more negative. This is the opposite of the expected relationship. It was decided that the glass wall potential must be following the suppressor voltage at low pressures, thereby allowing stronger electron cloud oscillations to develop. This was checked and found to be true. Placing the glass wall at filament potential, by making contact with the metal film

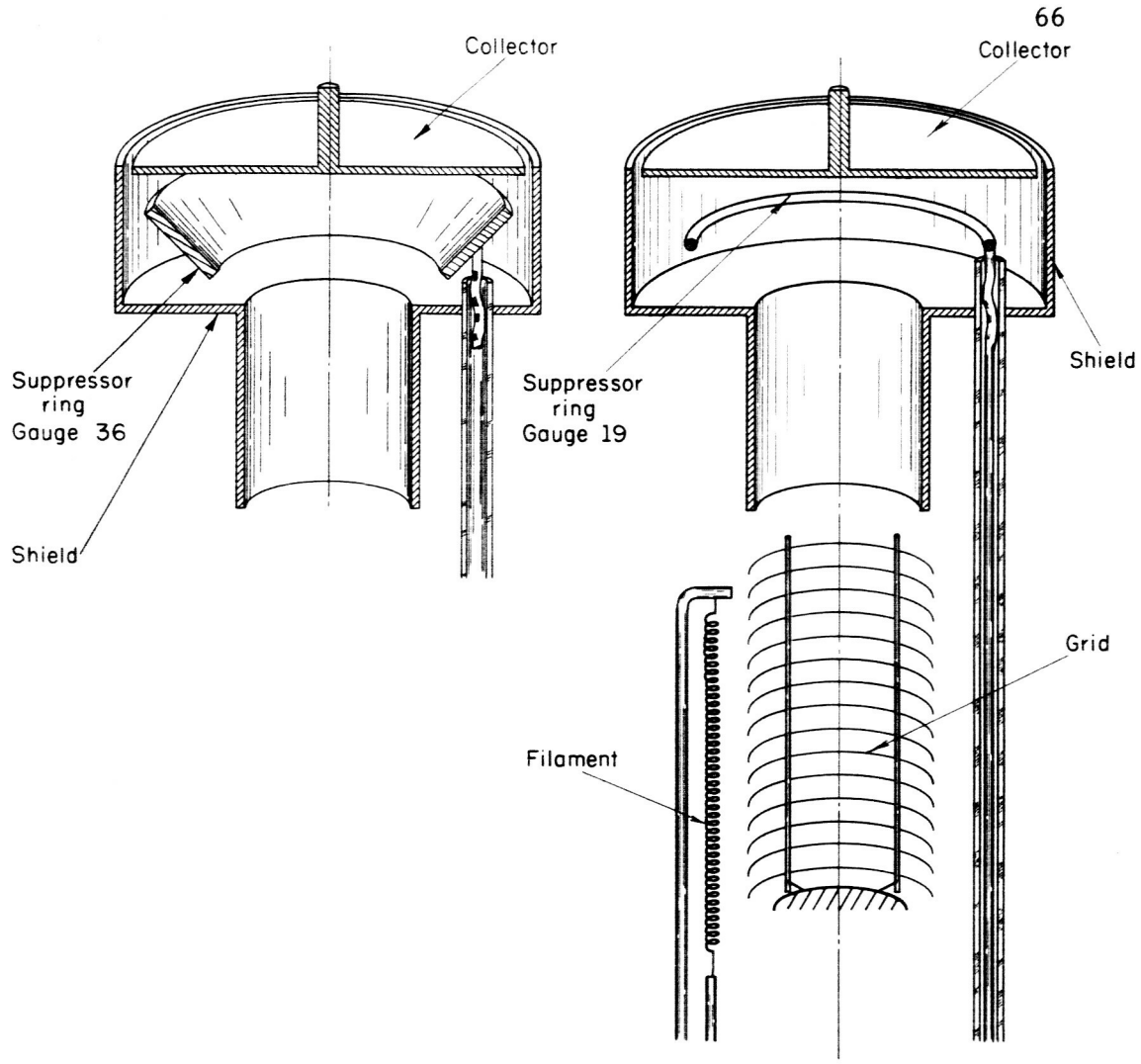

Fig. 6.4. Cutaway Drawing of Suppressor Gauge Showing Change in Suppressor Geometry.

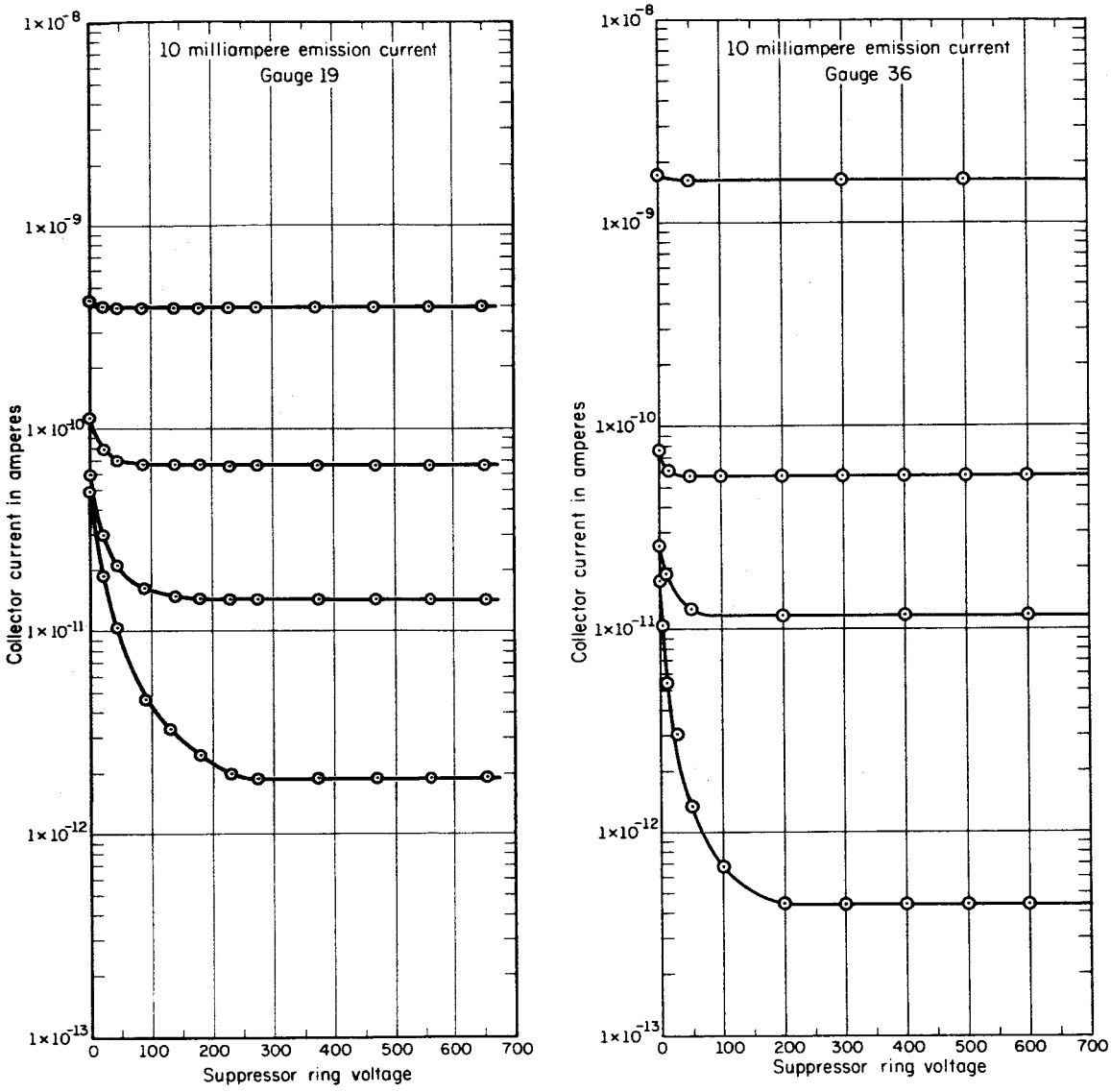

Fig. 6.5. Collector Current versus Suppressor Voltage at Different Pressures for the Older and Newer Models of the Suppressor Gauge.

which exists on the wall as the result of outgassing the grid, eliminated the oscillation. Similarly oscillations in Bayard-Alpert gauges have been found to drive the walls of the gauge negative, and also in this case fixing the wall potential at filament potential eliminated the oscillation.

6.4 Davis & Vanderslice Mass Spectrometer

We have finally obtained a working Davis and Vanderslice mass spectrometer. We feel that it is ready to be used in an experiment but have not yet decided what the experiment will be.

7. PLASMA PHYSICS

M. Raether
J. K. Aggarwal
A. Barger
H. Bohmer
W. Carr
J. Crowder
B. Hicks
T. Lie
C. Mendel
H. G. Slottow
M. A. Smith
R. Hosken

7.1 Linear Plasma Induction Accelerator

A linear plasma betatron has been built in an effort to study electron runaway in a strong electric field. It should have several advantages over the circular plasma betatrons built at other institutions.* The main advantages are the lack of orbit conditions, so that a diffuse velocity spectrum can be accelerated, and larger electric fields.

The device (Fig. 7.1) is essentially a transformer with (in our case) four primaries, and one secondary. The secondary circuit is completed by the plasma. The primaries each are supplied by three 2.5 μfd fast discharge condensors which can be charged to as high as 20 KV. Switching is done by ignitrons, and low inductance coaxial cable is used to complete the circuit. This circuit can supply about 50 KV with an impedance of 0.2 ohm to the plasma, with a quarter cycle of about 2 μsec. Fig. 7.2 shows a schematic of the firing circuit.

The discharge takes place in a ceramic tube which is 16 inches long and 1 inch inside diameter. It is physically situated in the center of the transformer. The gas in the tube is preionized by a D.C. discharge between the end electrodes and a center ring. Hydrogen and helium gases are to be used at pressures of 10 to 100 microns.

---

* Stevens, Bonn, CERN

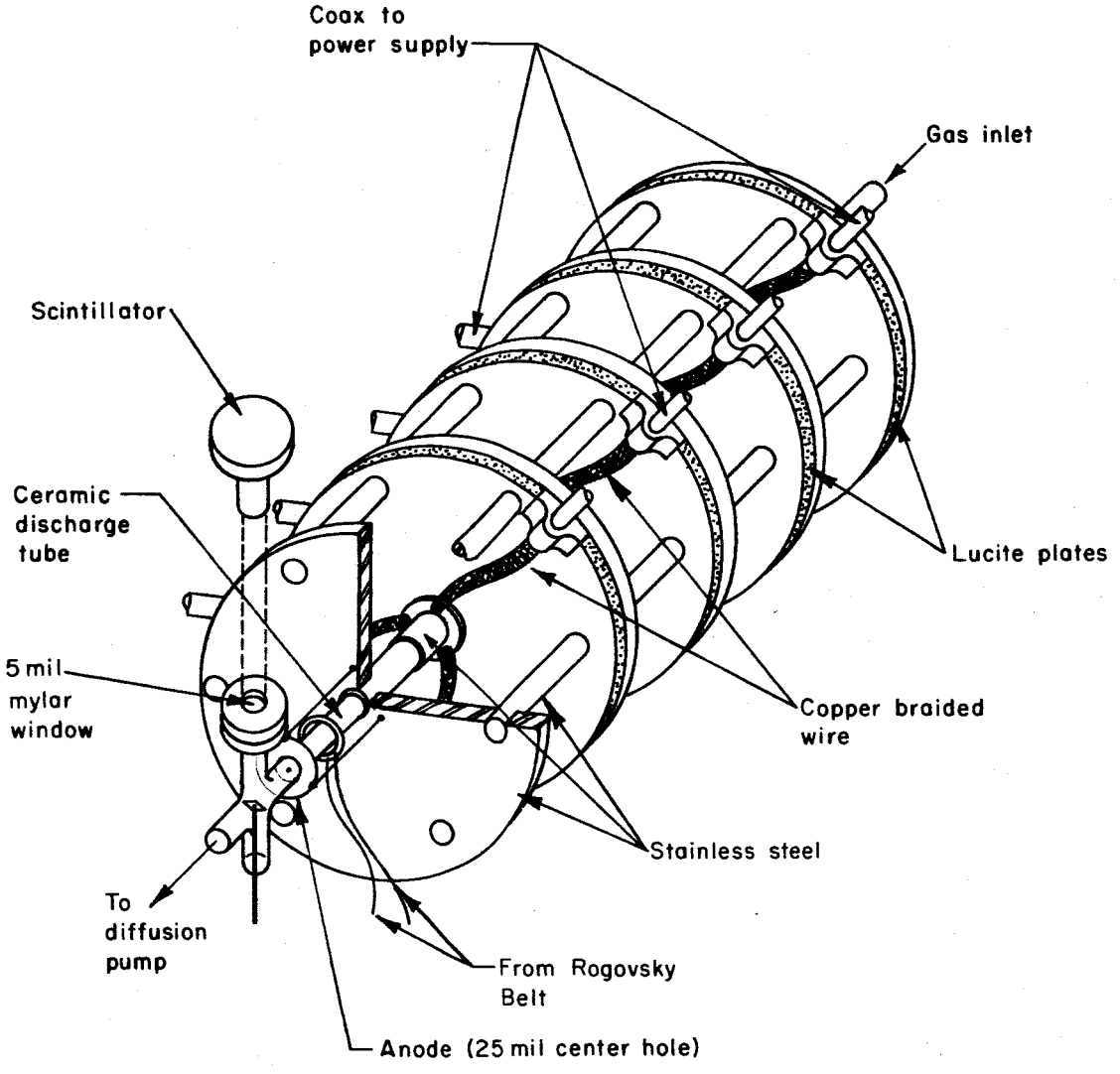

Fig. 7.1. Schematic of Linear Induction Accelerator.

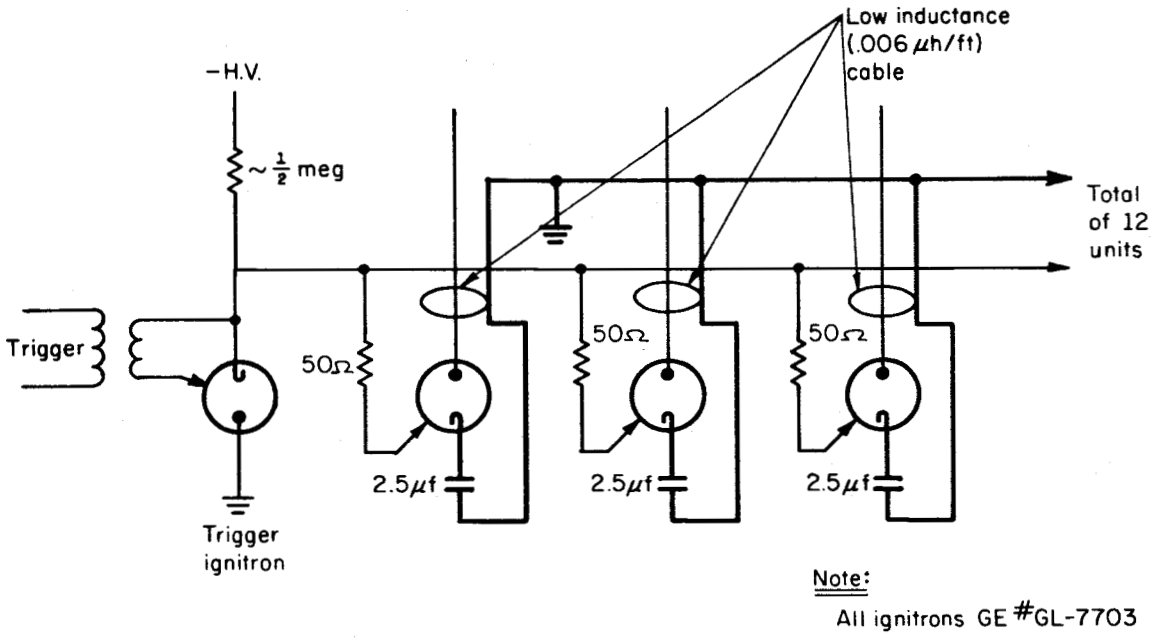

Fig. 7.2. Firing Circuit for Linear Induction Accelerator.

The potential across the tube and current in the tube are monitored by magnetic probes and Rogovsky coils. A small (25 mil) aperature at the anode allows the electrons to pass into an evacuated area where they hit a tungsten target and produce x-rays. The x-ray production is measured by a scintillation counter. Fig. 7.3 shows a photograph of the apparatus.

The device is now complete, and experimental results shall shortly be obtained. Particular attention will be paid to the interaction of the run-away electrons with plasma oscillations, originating from instabilities. Calculations of this interaction mechanism, using the quasi-linear theory, are being persued in parallel to the experiment.

C. Mendel
M. Raether

7.2 Incoherent Scattering

During the past quarter, a new LEL mixer-amplifier was obtained. The IF frequency is 240 mc with a 20 mc bandwidth. This has improved the receiver sensitivity by a factor of 20. Fig. 7.4 shows the receiver sensitivity at 9500 mc. In addition the frequency variation is much smaller than with previous systems.

A series of runs were made to determine how the scattered signal varies with gas pressure and discharge current. Fig. 7.5, 7.6, and 7.7 show plots of scattered power versus discharge current for pressures of .65, .80, and .90 mm Hg. respectively. For these graphs the incident frequency was 8480 mc. and the local oscillator frequency was 9985 mc. Only the lower sideband was allowed into the mixer, so the receiver frequency was 9745 mc.

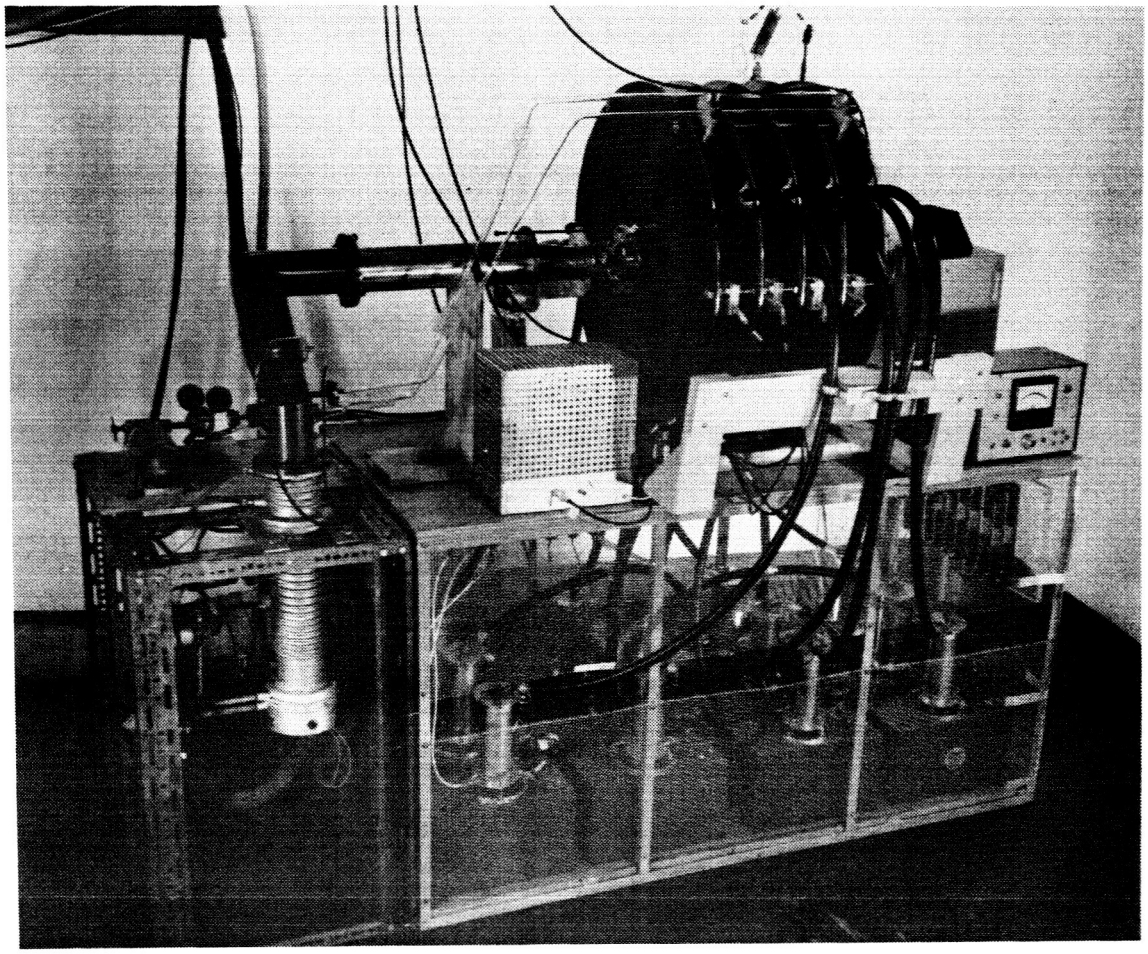

Fig. 7.3.

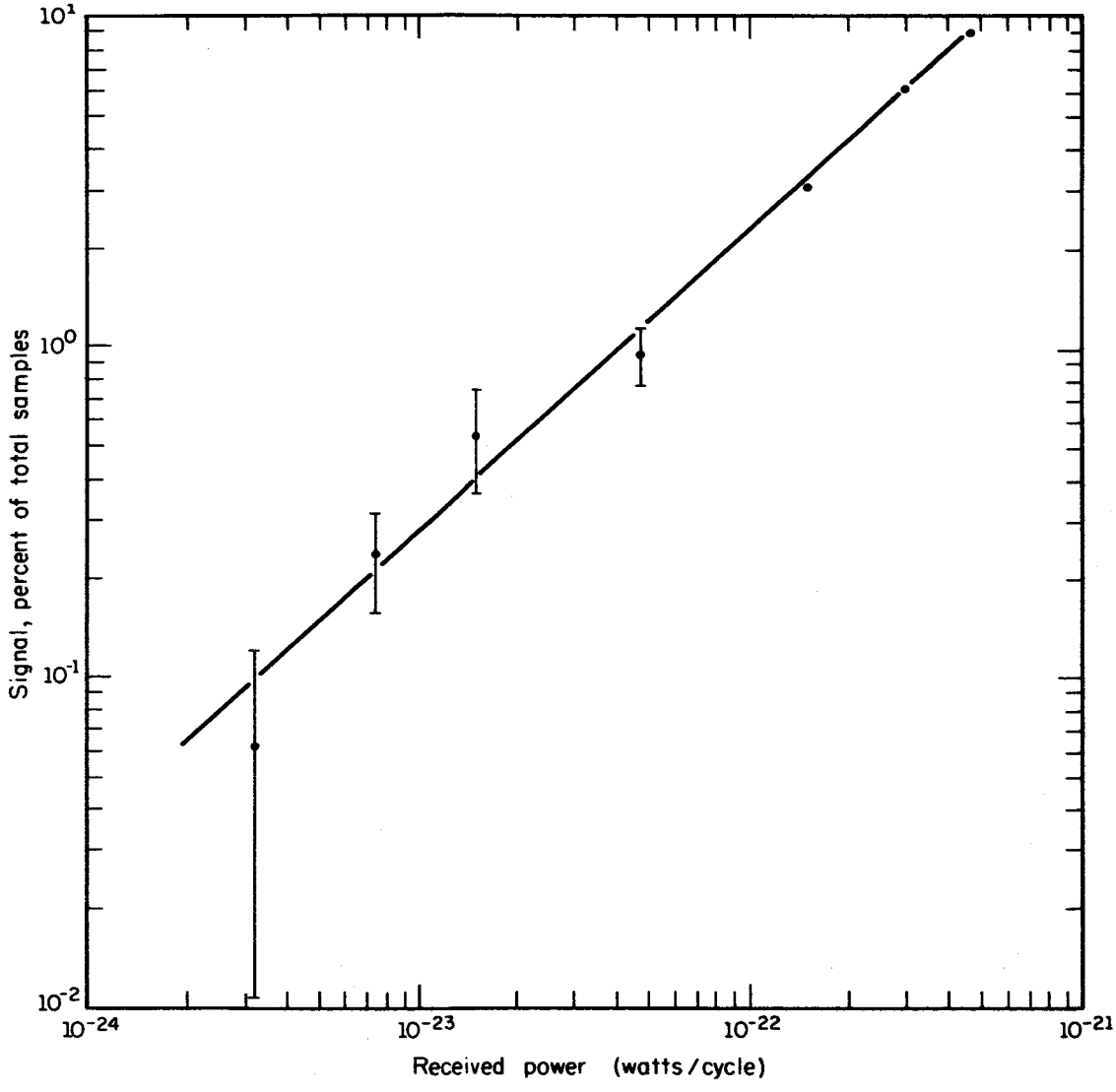
10^1
10^0
10^{-1}
10^{-2}
Signal, percent of total samples
10^{-24}
10^{-23}
10^{-22}
10^{-21}
Received power (watts/cycle)

Fig. 7.4.

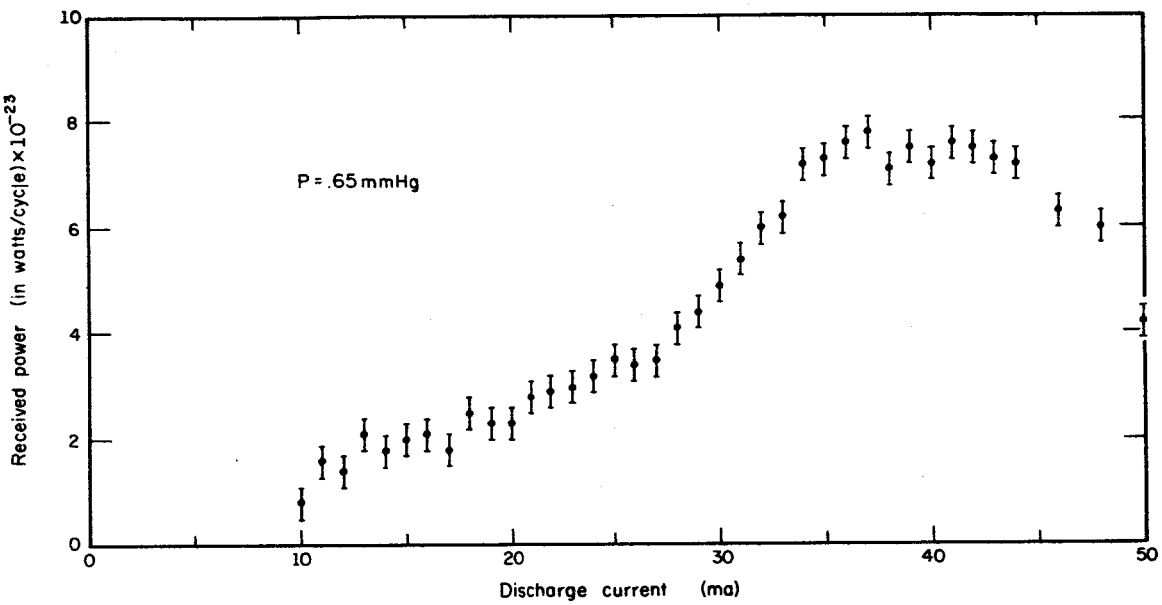
P = .65 mmHg
Received power (in watts/cycle) x 10^-23
Discharge current (ma)
0
2
4
6
8
10
0
10
20
30
40
50

Fig. 7.5.

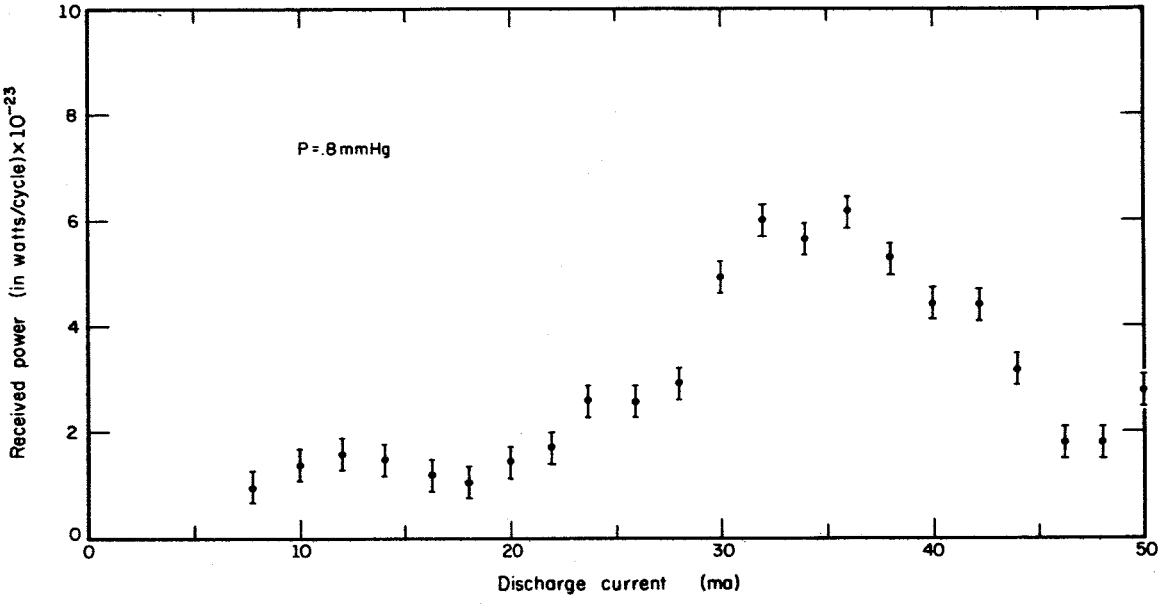
P=.8mmHg
Received power (in watts/cycle)×10⁻²³
Discharge current (ma)
0
2
4
6
8
10
0
10
20
30
40
50

Fig. 7.6.

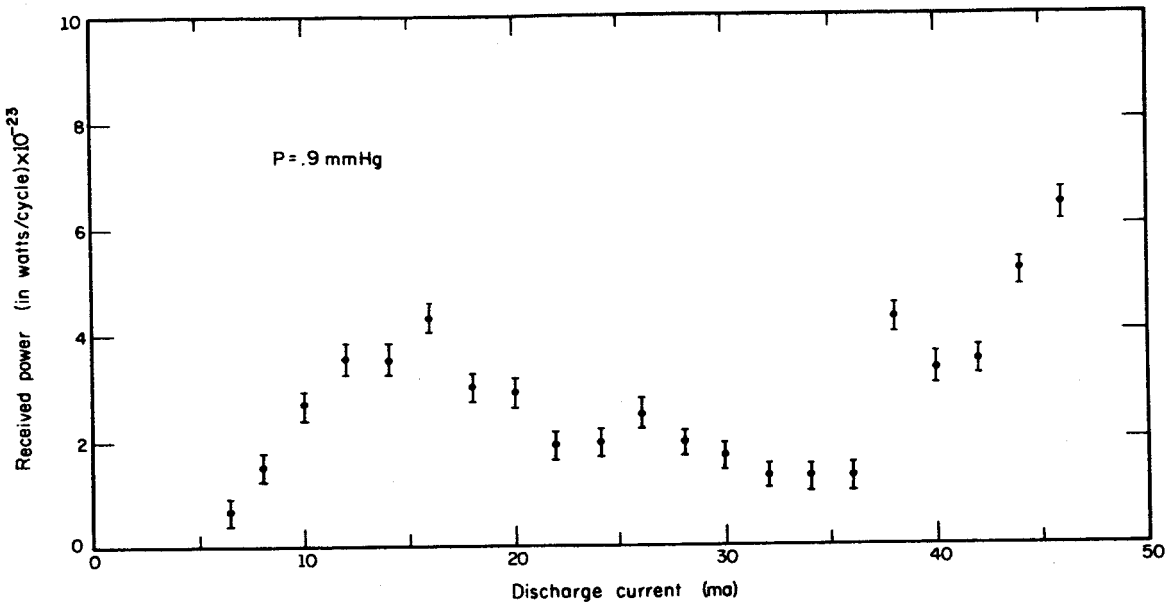
P=.9 mmHg
Received power (in watts/cycle)×10⁻²³
Discharge current (ma)
0
2
4
6
8
10
0
10
20
30
40
50

Fig. 7.7.

In Fig. 7.5 there is a broad peak at 38 ma. and a small peak at approximately 12 ma. In Fig. 7.6 the large peak has shifted to 33 ma. and decreased in size, and the small peak has remained stationary and increased slightly in size. In Fig. 7.7 the high frequency peak has nearly disappeared while the low peak has become still larger. In addition there is a sharp rise at high current due to modulated noise.

We have tentatively identified these peaks to be due to scattering from oscillations of the discharge column of a type similar to the Tonks-Dattner resonances.

W. Carr
H. Böhmer
M. Raether

7.3 The Boltzmann Equation

We have developed (in collaboration with Professor Yen of the Department of Aeronautical and Astronautical Engineering) a new and purely algebraic theory of shock wave structure. The theory provides a framework for making sensitive comparisons between Mott-Smith and Monte Carlo results, comparisons which are needed to understand the convergence properties of our overall method for solving the Boltzmann equation. The theory also can make predictions of shock structure for any monatomic gas described by its coefficients of viscosity and of heat conductivity on the cold and hot sides of the shock. Programs making use of each capability of the theory are being written. In particular, the range of Mach number for which the theory is valid will be determined.

Production runs were completed for five values of Mach number (from 1.8 to 4.0), using five stations, 40,000 collisions and 15

iterations. New programs finished in this quarter will permit calculations up to a Mach number of 8 or 10 and will provide the values of more than 30 new functions which can be used to characterize our iterative method of solution and to compare with analytical theories like the "algebraic" one mentioned above.

A proposal was submitted to NASA in April for a research grant in support of our studies of the kinetic theory of shock waves.

B. Hicks

8. HIGH MAGNETIC FIELD SUPERCONDUCTORS

C. B. Satterthwaite
J. O. Kopplin
W. O. Gentry
I. Toepke
R. Bernstein
R. Ries
R. Klingbiel
L. Edelheit
M. G. Craford*

8.1 Introduction

This group is primarily interested in studies which contribute to an understanding of the persistance of superconductivity to very high magnetic fields. Studies include materials preparation, investigations of the properties of Type II superconductors and the properties of superconducting specimens of very small dimensions.

8.2 Magnetization Studies of Type II Superconductors

Completion of the study of vanadium as a type II superconductor still awaits the procurement of reasonably pure materials. Dr. Sell of Westinghouse has been cooperating with us in trying to produce pure V single crystals by electron-beam zone refining. To date the results have been disappointing in that residual resistance ratios ($R_{300^oK}/R_{4.2^oK}$) are no greater than earlier specimens (i.e., less than 20). Other sources of pure material are being investigated.

Measurements on pure Re in the form of pure single crystal ($R_{300}/R_{4.2}$= 2000) and annealed wire indicate that pure Re is a superconductor of the first kind, i.e., shows a complete Meissner effect at magnetic fields below H_c and no diamagnetism above.

R. Ries
C. B. Satterthwaite

*Working on joint project with Thin Film Group

8.3 Crystallization of Nb_3Sn

Several small crystals have been grown during three runs of the Nb_3Sn furnace in the later part of this report period. These were the initial runs using the recently installed magnetic stirring system and temperature control for the Nb-Sn solution with limited independent temperature control of the niobium tipped probe.

Although no detailed analysis of the crystals has as yet been carried out, several of the crystals appear to have nearly perfect structure. This is in contrast to the rather imperfect structure of the Nb_3Sn crystals grown in the initial phase of this investigation. Due to the fact that it has been necessary to make minor changes in the furnace following each run, it has been impossible to correlate the crystal structure obtained with the various furnace parameters. A series of runs is planned which will allow relationships to be established between crystal structure, size and growth rate and the various furnace parameters.

The investigation of the possibility of iodometric determination of tin in low concentrations using the spectrophotometric isolation procedure has been continued. This study has developed into a search for a reductor for the stannic solutions which will not precipitate as the hydroxide at a pH sufficiently high to minimize the photo-oxidation of iodine to iodide, not produce a colored solution adding to the ultraviolet absorption, or not react with the iodine in the neutral or slightly acidic solutions required for the spectrophotometric determination. Hypophosphite, bismuth amalgam, cadium, lead and nickel were all studied as possible reductors; however, all of these failed for one or more of

the above stated reasons. Nickel was investigated quite thoroughly as a possible reductor. This included shifting the wavelength isolated by the spectrophotometer in hopes of increasing the sensitivity to the triiodide and decreasing the sensitivity to the broad nickel chloride absorption band. Complexation of the nickel was tried but again there was excessive overlapping of the absorption bands. The nickel absorption band was measured separately in an attempt to compensate the error due to the nickel interference, but this was unsuccessful for the large nickel concentrations required for the complete reduction of the tin.

The results of this investigation indicate that if a suitable reductor can be found, the spectrophotometric isolation procedure is sufficiently sensitive for the determination of microgram tin concentrations. No other method for the accurate quantitative chemical determination of tin in low concentrations has been reported, and thus the problem remains. This investigation has at least been temporarily terminated because Mr. Lanier has completed his requirements for the Ph.D degree in chemistry and has left the University.

J. O. Kopplin
R. Klingbiel
W. Lanier

8.4 Electron Depairing and Tunnelling in Superconductors

A program was described in the last QPR to study the change in the energy gap of a superconductor due to a drift velocity of the superconducting electrons (i.e., a supercurrent). Preliminary studies of the tunnelling characteristics between niobium foils and indium films through a layer of niobium oxide have (a) demonstrated that one can measure, quite accurately, the energy gap in an indium film (as desired

for the depairing experiment) and in the niobium by this methos and (b) revealed what are believed to be some yet unreported aspects of the supercurrent tunnelling between two superconductors (Josephson Effect).

(a) A typical tunnelling curve (I vs. V) for the niobium-indium is shown in Fig.8.1. It has been theoretically rationalized and experimentally demonstrated that the sharp cusps occur at $\pm(\mathcal{E}_2 - \mathcal{E}_1)$ and the points of steepest ascent at $\pm(\mathcal{E}_2 + \mathcal{E}_1)$ where $\mathcal{E}_2$ and $\mathcal{E}_1$ are the energy gap parameters for the two superconductors. From a series of measurements of the type shown in Fig. 8.1, at temperatures ranging from $1.2^{o}K$ to the transition temperature of indium, the energy gap ($2\mathcal{E}$) for both indium and niobium were obtained. Fig. 8.2 shows a comparison of the energy gap for indium determined from tunnelling measurements together with the predictions of the B.C.S. (Bardeen, Cooper, Schrieffer) theory. The data for a similar comparison for niobium are not available because we are not equipped to control or measure temperatures above $5^{o}K$. The energy gap in the indium film is the quantity in which we are primarily interested for studying the phenomenon of depairing.

(b) Josephson predicted in 1962 that it should be possible for superconducting electron pairs to tunnel from one superconductor to another through an insulating barrier, thus one should see a tunnelling current at no voltage. He also predicted that the D.C. current should occur only at zero voltage, and that at finite voltage an AC supercurrent should flow of frequency $\nu=eV/h$ when e is the electronic charge, V is the voltage drop across the insulator and h is Plank's constant. The D.C. Josephson effect has been observed experimentally and some indirect experimental evidence exists to support the A.C. prediction.

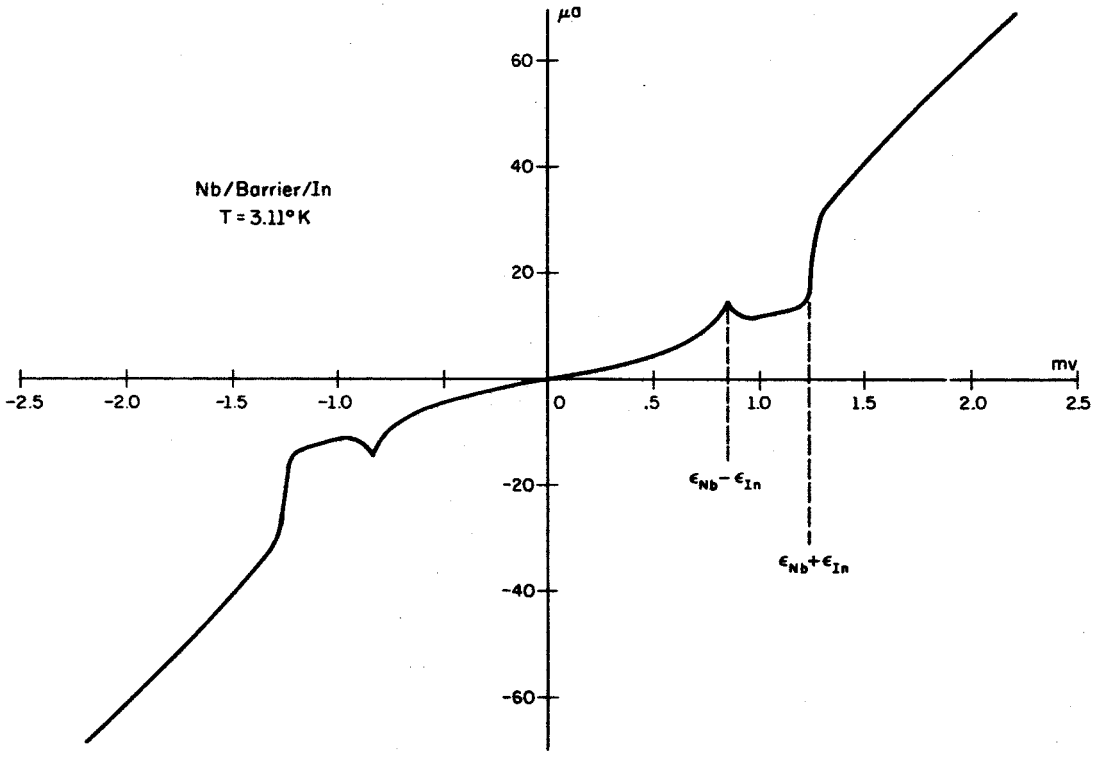

Fig. 8.1. Typical Tunnelling Characteristic (I vs V) for a Sandwich of Nb - Nb oxide - In.

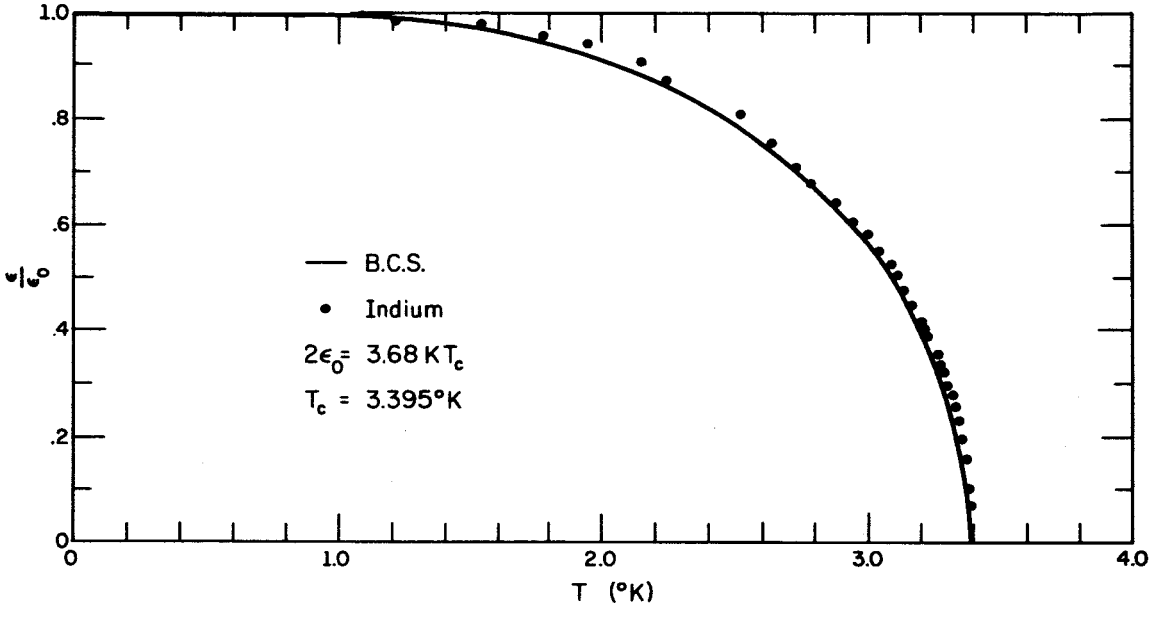

Fig. 8.2. Superconducting Energy Gap in Indium as a Function of Temperature Determined from Tunnelling Experiments and Comparison with Theory.

In the course of measurements just reported, we observed a D.C. Josephson effect and proceeded to study it with some care. In particular, we reduced the resistance of our tunnelling circuit so that we could observe a high negative resistance in the tunnelling junction. We were thus able to observe the region between V = 0 and the point where the normal tunnelling current rises steeply. Fig. 8.3 shows the characteristic observed by us in comparison with Josephson tunnelling curves reported in the literature. The DC current peaks at finite voltage were completely unexpected and are yet unexplained.

A crude coil was constructed around the specimen and the magnetic field varied in its vicinity. Fig. 8.4 shows how the characteristic changes as a function of field. Magnetic field is indicated by milliamps through the coil and is approximately 3 gauss per amp. The earth's field was not cancelled.

Attempts are now being made to reproduce the results with another specimen and study the effect in a controlled magnetic environment.

R. Ries
M. G. Craford
R. N. Peacock
C. B. Satterthwaite

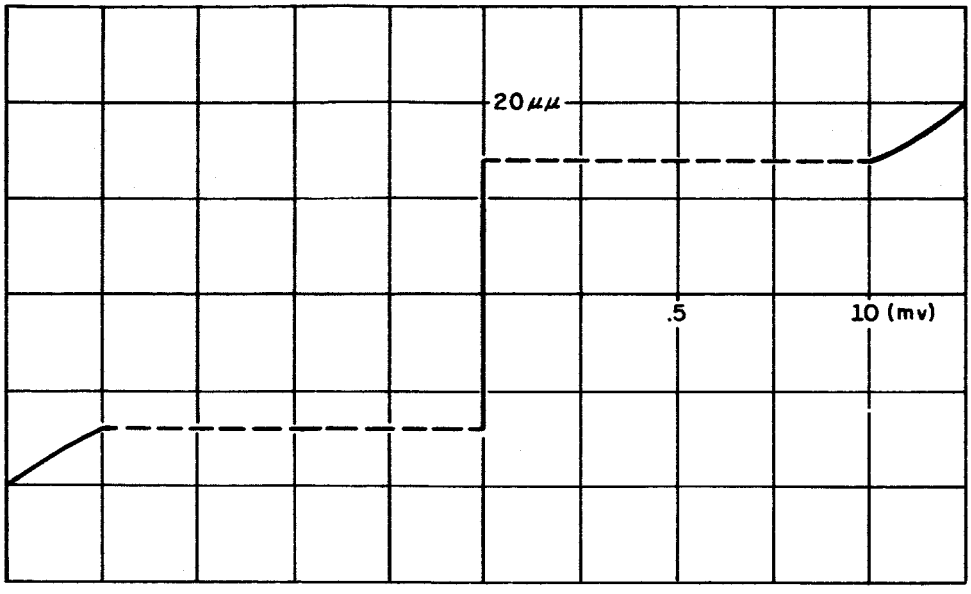

DC Josephson Tunnelling as Observed by Standard Techniques Reported in the Literature

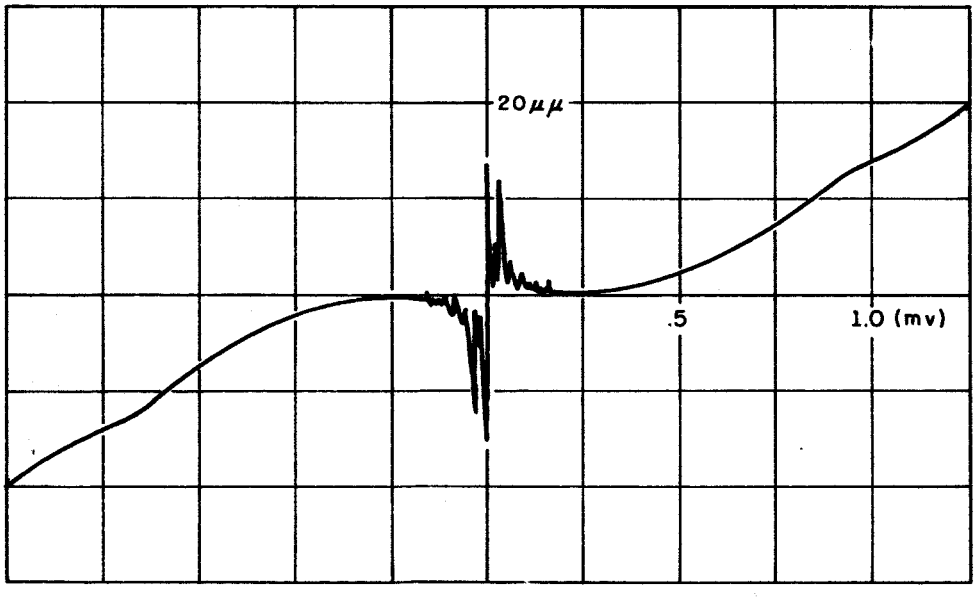

Fig. 8.3. DC Josephson Tunnelling and Associated Structure Observed with New Low-Resistance Tunnelling Circuit.

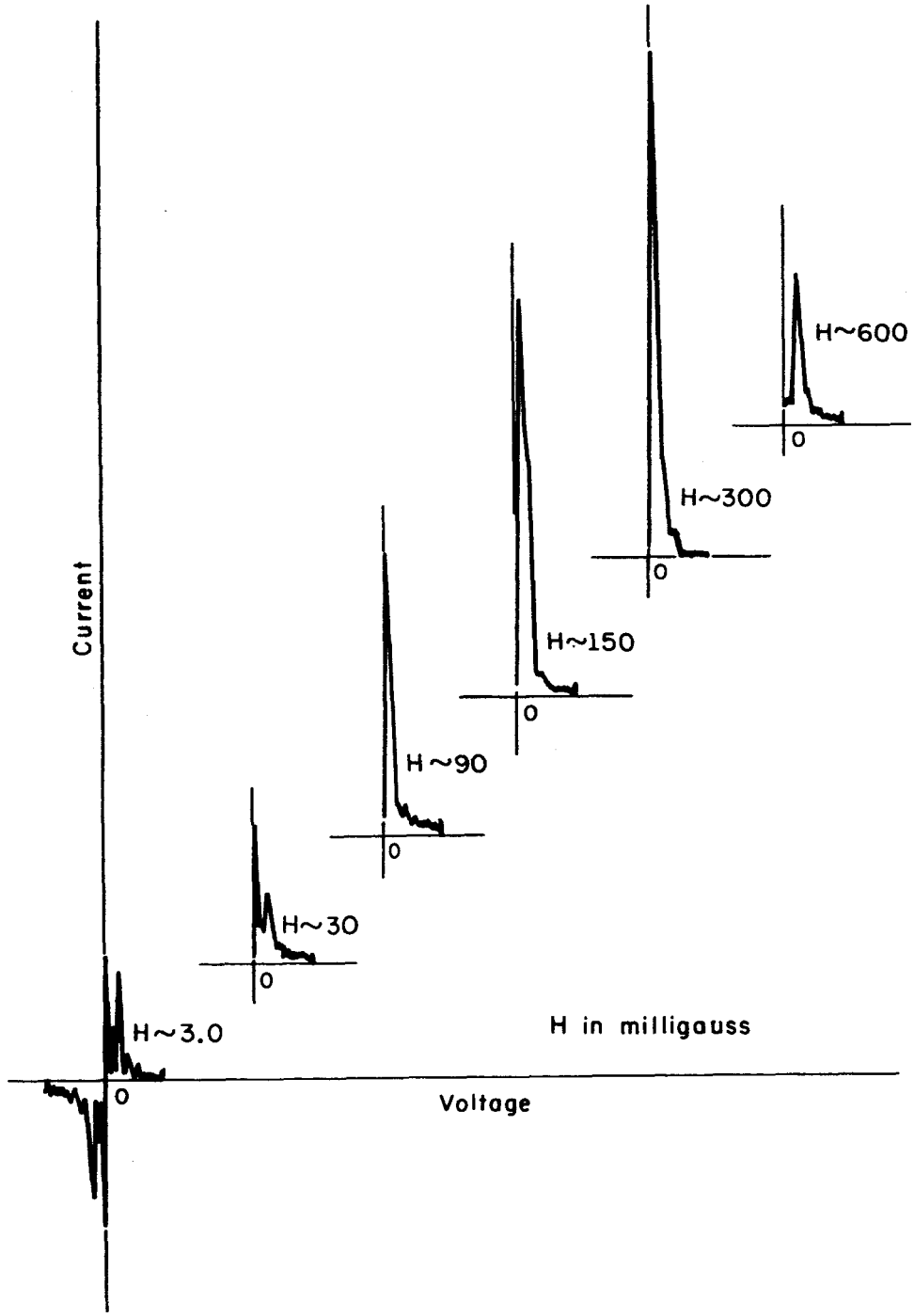

Fig. 8.4. Variation of the Tunnelling Characteristic as the Magnetic Field Parallel to the Junction was Varied. Absolute value of the magnetic field is uncertain by at least the earth's field.

9. HIGH VOLTAGE BREAKDOWN

D. Alpert
T. Casale
D. Lee
E. M. Lyman
H. Tomaschke

Additional work has been done on the study of field-emission characteristics of tungsten using a modified field-emission microscope. This instrument is similar in design to the Mueller field emission microscope in which the field-emitted electrons from the cathode impinge on a luminescent screen thereby displaying a pattern of the emission sites. However, instead of using the normal type of cathode which is a very fine, single crystal point ($\sim 10^{-5}$ cm in radius), the cathode used in this instrument is the blunt end of a tungsten wire 7.5×10^{-3} cm in diameter. This wire is mounted on a filament so that it can be heated to smooth out some of the sharper points formed on the end of the wire during the construction of the cathode.

The emission patterns obtained with this microscope typically consist of a few (ten or less) regions which are more or less uniformly illuminated. Within these regions, small spots are often observed to flicker on and off. These flickers are accompanied by current fluctations and rectangular pulses[1]. The cause of this flickering has not been clearly established. However, it has been observed that the rate of flickering increases if the gas pressure in the system is increased or if the dc level of the emission current is increased. This suggests a mechanism associated with ion bombardment of the cathode.

---

[1] C.S.L. Progress Report, Dec. 1963 - Feb. 1964.

Cooling the cathode to liquid helium temperature has little effect on the flickering.

Plans are being made to study the flickering spots in more detail. One technique which will be tried is the observation of the light from the spots with a photomultiplier or similar device. Also, cathodes will be made from "ultrapure" tungsten wire to see if this changes the flickering characteristics.

H. Tomaschke

10. EVAPORATED THIN FILMS

R. N. Peacock
M. G. Craford
J. T. Jacobs
R. E. Zelac
G. Riddle
A. Jones

10.1 Properties of Tin Oxide Films

Proposed use of tin oxide films on glass, either as conducting films or as secondary emitters, has made it seem worthwhile to measure characteristics of such films. While studying the temperature coefficient of resistance, it became evident that the films were unstable at temperatures greater than 300°C. This suggested that a study of the effects of different ambient gases at constant high temperature would give valuable information about the properties of tin oxide films.

Thin films of tin oxide may be produced by several techniques.[1,2,3] The technique which was used for preparing the films is similar to that used by Gomer[3]. This method is likely to produce a film with a deficiency of oxygen atoms,[2] i.e., an excess of tin ions. This implies that the film is n-type. When the sample is heated in oxygen, it can be expected to approach stoicheometry due to diffusion of the oxygen into the film.

There is a surface layer of bound oxygen atoms and the corresponding charge within the film itself. This causes the conduction band near the surface to be further away from the Fermi level, hence the conductivity near the surface is lower.

---

[1] R. E. Aitchison, Aust. J. Appl. Sci., 5, 10 (1954).

[2] Libby-Owens-Ford Glass Co., and McMaster, H. A., Brit. Pat. #632,256 (Oct. 1942); #671,767 (April 1949); #686,280 (Dec. 1949); #682,342 (July 1949).

[3] R. Gomer, Rev. Sci. Instrum., 24, 993 (1953).

If the oxygen atmosphere is replaced by an inert gas at a temperature sufficiently high that the oxygen will desorb, the surface is freed of the adsorbed layer. Partial removal of the adsorbed oxygen causes a decrease of the space charge in the film. This lowers the conduction band with respect to the Fermi level. Hence the conductivity is decreased. Passing forming gas (90% N, 10% H_2), over the sample at elevated temperatures will cause the adsorbed oxygen to unite with the hydrogen in the forming gas to form water. In addition, some reduction of SnO_2 will occur. This process leaves an excess of tin in the film. It is also very probable that some of the nitrogen present in the forming gas is weakly adsorbed to the surface of the film. The final effect of this reaction is to cause the resistance of the film to decrease. Similar effects have been noticed in zinc oxide.[4]

Several measurements in air of resistance as a function of time were made at approximately 400°C. Tubular pyrex and flat lime glass substrates were used. Both types of samples yielded similar results.

A plot of the resistance at constant temperature as a function of time for a tubular sample heated in air is given in Fig. 10.1. The initial and final resistances were 656 ohms and 56,000 ohms, respectively. Upon cooling from 400°C to room temperature, the resistance went from 10,000 ohms to 56,000 ohms.

Next the ambient gas was changed while the sample was at an elevated temperature. The samples were brought to temperature in argon.

---

[4] J. T. Okada, Phys. Soc. of Japan, 10, 1110 (1957).

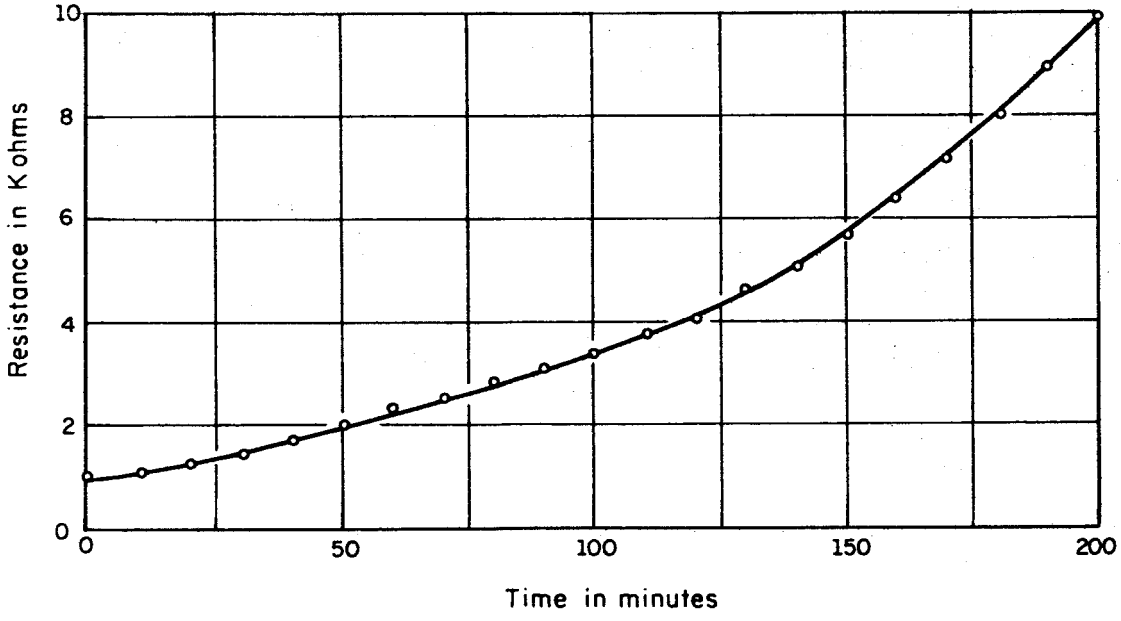

Fig. 10.1. Resistance versus time for a tin oxide film in air at $391 \pm 5^{\circ}$ C.

After the tests were completed, the temperature was lowered while the sample was again in an argon atmosphere.

Another sample was annealed for three hours at 620°C after formation. Although this sample was very sensitive to different gases at high temperature, as is described later, the over-all change in resistance at room temperature was very slight indeed. The initial sample resistance was 573 ohms. The final resistance was 537 ohms. This corresponds to an over-all change of 6.3%. It was also noticed for this sample as well as others, that the films in argon seemed to have a small positive temperature coefficient from 420°C to 30°C.

The first change of ambient gas was from argon to oxygen. Upon admission of oxygen, the resistance increased from 545 ohms to 1650 ohms in less than 10 seconds. In 80 seconds, it was 1800 ohms; in 11 minutes it stabilized at 1890 ohms. Upon readmitting argon, the sample's resistance decreased in an exponential fashion to 690 ohms. The time constant for this change was approximately 11 seconds.

Forming gas was next admitted to the sample. The results as shown in Fig. 10.2 are surprising. A sizable but brief increase in resistance may be noted. Another similar test is shown in Fig. 10.3. Such peaks were not observed in a subsequent test when forming gas was substituted directly for oxygen.

In some cases an instantaneous decrease in sense opposite to that expected was noticed when gases were changed. For example, when oxygen was admitted to a sample which was previously in argon, the resistance increased very rapidly.

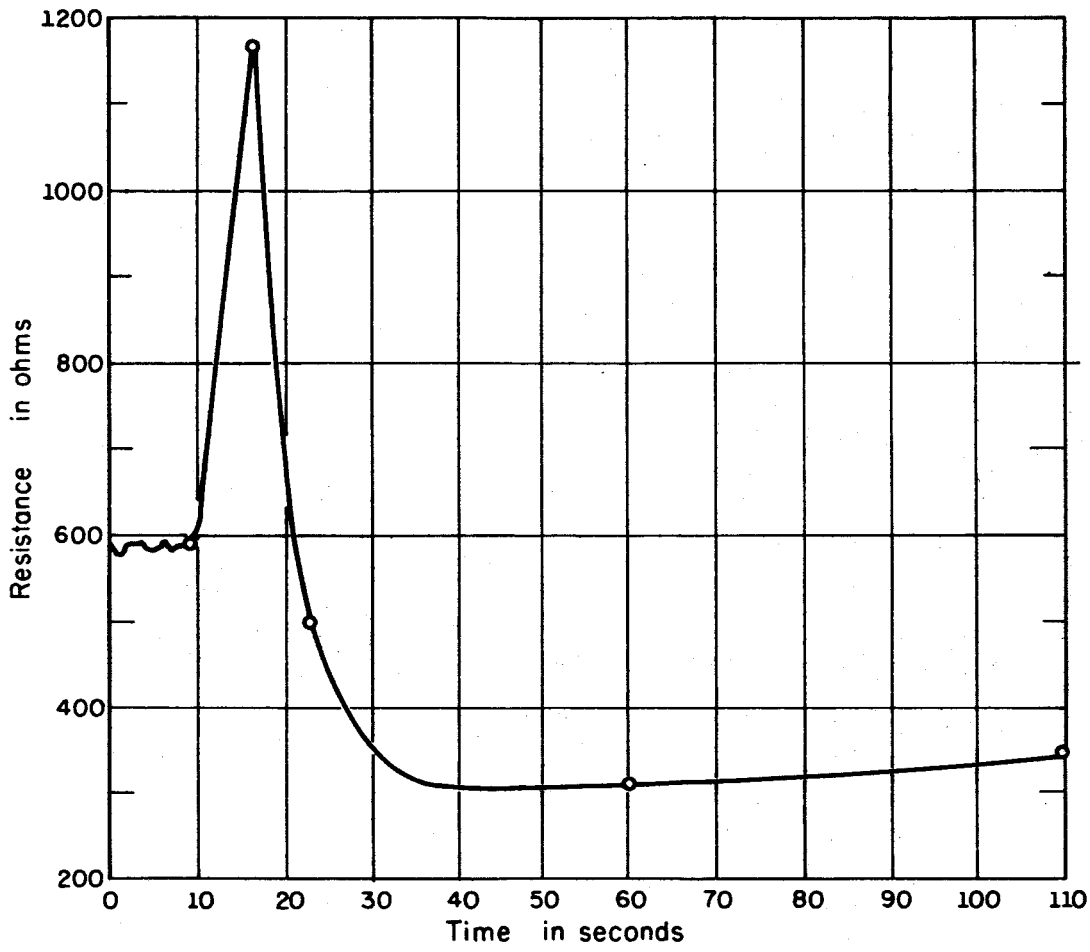

Fig. 10.2. Resistance versus time for a tin oxide film during a change of the ambient gas from argon to forming gas. Forming gas introduced at time = 10 seconds.

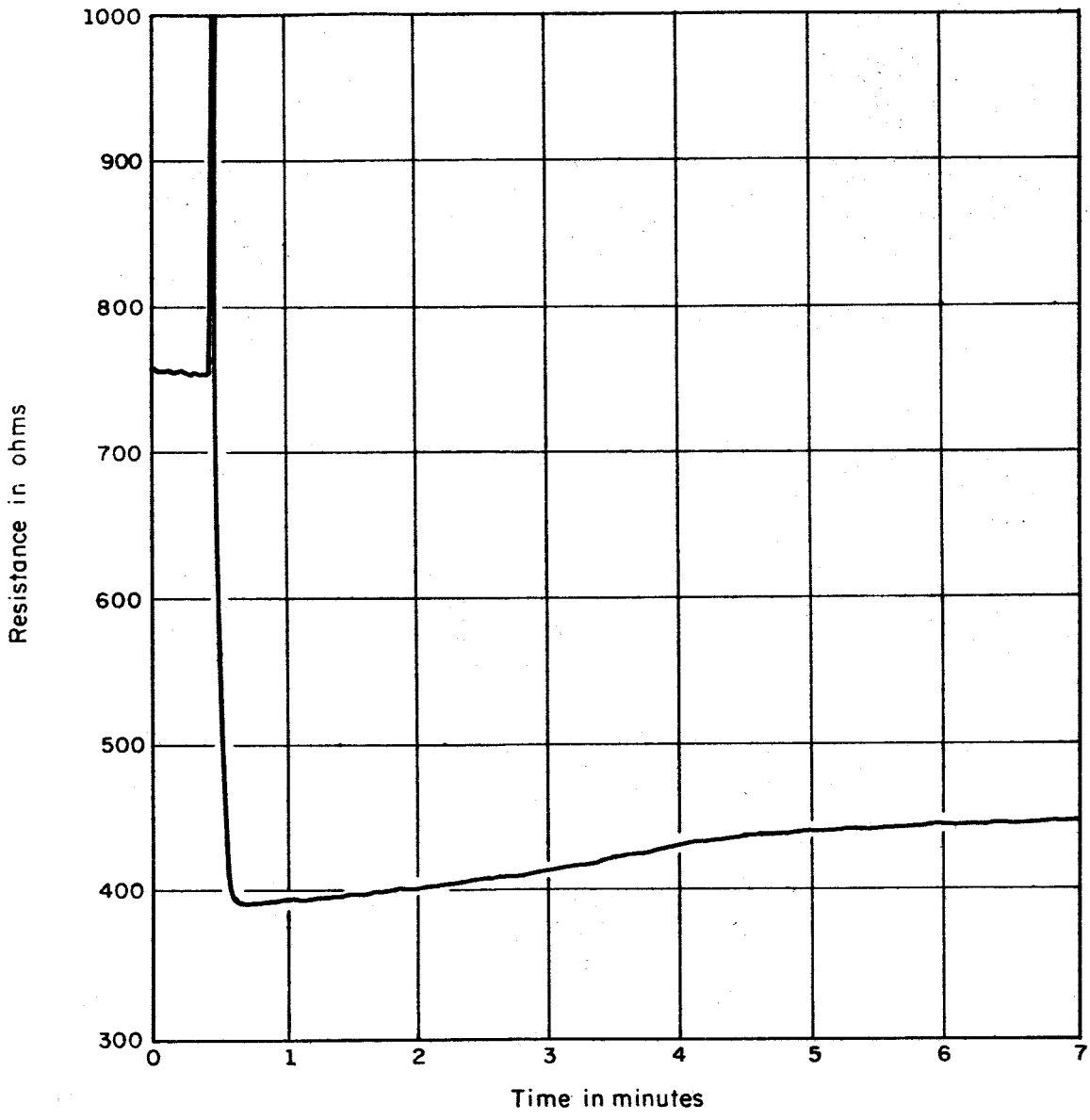

Fig. 10.3. Resistance versus time for a tin oxide film during a change of ambient gas from argon to forming gas. Change of gas occurred at time = .4 minutes.

Similar experiments were conducted at room remperature. In this case there was no noticeable change in the resistance when the ambient gas was changed.

The positive temperature coefficient of resistance for the tin oxide is as yet unaccounted for. Such behavior might be related to the surface states. The presence of argon whould not alter the conduction properties of the film. When a tin oxide film is heated in argon, the surface may be a monomolecular layer of tin. If this is true, then this layer would dominate the conduction process. In this case the sample would have a positive temperature coefficient.

The changes in resistance at constant high temperature when the ambient gas is changed indicated that the samples are unstable. The very fast responses, i.e., responses that occur in times less than 10 seconds, are likely due to changes in surface states. The changes which are very slow are probably linked with either a bulk effect, i.e., deeper in the sample, or slow reactions.

Further studies of the electrical properties of tin oxide films are now underway.

J. T. Jacobs
R. N. Peacock

10.2 Hard Superconducting Films

Several vanadium films were made and measured. The Varian Associates electron-beam source was used in the VI-4 evaporator with pressures around 10^{-7} Torr. Lime glass microscope slides were used as substrates, but unfortunately no control of substrate temperature during deposition was possible. The superconducting properties were very poor,

since the resistive transition for the films occurred at about $2^{o}K$, instead of $5.1^{o}K$ as expected for pure annealed bulk material. This must mean that the films are impure, highly strained, or both.

George Riddle

10.3 Vacuum System for Deposition of Epitaxial Films

The vacuum system for studies of film growth has been tested at pressures as low as 10^{-9} Torr. The pumping system combines a slow diffusion pump with zeolite trap and a Varian Associates titanium sublimation pump. Successful operation of the titanium pump has been achieved, and it is expected that lower pressures will be reached as the work progresses. The liquid nitrogen capacity of the substrate holder has been found adequate to maintain substrates at low temperatures for periods sufficient to deposit films. The system is presently being prepared to form tin films on single crystal NaCl substrates.

R. E. Zelac